

Reliable performance. Learn how we do it.  
Reproducible results.



## The RNA-Binding Proteins Zfp3611 and Zfp3612 Enforce the Thymic $\beta$ -Selection Checkpoint by Limiting DNA Damage Response Signaling and Cell Cycle Progression

This information is current as of November 6, 2017.

Katharina U. Vogel, Lewis S. Bell, Alison Galloway, Helena Ahlfors and Martin Turner

*J Immunol* 2016; 197:2673-2685; Prepublished online 26 August 2016;  
doi: 10.4049/jimmunol.1600854  
<http://www.jimmunol.org/content/197/7/2673>

**Supplementary Material** <http://www.jimmunol.org/content/suppl/2016/08/26/jimmunol.1600854.DCSupplemental>

### Why *The JI*?

- **Rapid Reviews! 30 days\*** from submission to initial decision
- **No Triage!** Every submission reviewed by practicing scientists
- **Speedy Publication!** 4 weeks from acceptance to publication

*\*average*

**References** This article **cites 61 articles**, 27 of which you can access for free at:  
<http://www.jimmunol.org/content/197/7/2673.full#ref-list-1>

**Subscription** Information about subscribing to *The Journal of Immunology* is online at:  
<http://jimmunol.org/subscription>

**Permissions** Submit copyright permission requests at:  
<http://www.aai.org/About/Publications/JI/copyright.html>

**Email Alerts** Receive free email-alerts when new articles cite this article. Sign up at:  
<http://jimmunol.org/alerts>

*The Journal of Immunology* is published twice each month by  
The American Association of Immunologists, Inc.,  
1451 Rockville Pike, Suite 650, Rockville, MD 20852  
Copyright © 2016 by The American Association of  
Immunologists, Inc. All rights reserved.  
Print ISSN: 0022-1767 Online ISSN: 1550-6606.



# The RNA-Binding Proteins Zfp3611 and Zfp3612 Enforce the Thymic $\beta$ -Selection Checkpoint by Limiting DNA Damage Response Signaling and Cell Cycle Progression

Katharina U. Vogel,<sup>\*,1</sup> Lewis S. Bell,<sup>†,1</sup> Alison Galloway,<sup>‡</sup> Helena Ahlfors,<sup>§</sup> and Martin Turner<sup>§</sup>

The RNA-binding proteins Zfp3611 and Zfp3612 act redundantly to enforce the  $\beta$ -selection checkpoint during thymopoiesis, yet their molecular targets remain largely unknown. In this study, we identify these targets on a genome-wide scale in primary mouse thymocytes and show that Zfp3611/12 regulate DNA damage response and cell cycle transcripts to ensure proper  $\beta$ -selection. Double-negative 3 thymocytes lacking Zfp3611/12 share a gene expression profile with postselected double-negative 3b cells despite the absence of intracellular TCR $\beta$  and reduced IL-7 signaling. Our findings show that in addition to controlling the timing of proliferation at  $\beta$ -selection, posttranscriptional control by Zfp3611/12 limits DNA damage responses, which are known to promote thymocyte differentiation. Zfp3611/12 therefore act as posttranscriptional safeguards against chromosomal instability and replication stress by integrating pre-TCR and IL-7 signaling with DNA damage and cell cycle control. *The Journal of Immunology*, 2016, 197: 2673–2685.

Early thymocyte development occurs in multiple quasi-discrete stages during which cells are required to pass through stringent developmental checkpoints. These checkpoints ensure TCR reactivity and prevent transformation into highly proliferative states. During the first stages of T cell differentiation in

mice, CD4<sup>-</sup>CD8<sup>-</sup> double-negative (DN) thymocytes can be subdivided into DN1–4 populations based on surface expression of CD44 and CD25 (1–3). The DN3 stage is further divided into DN3a and DN3b cells, the latter of which have successfully recombined the V, D, and J gene segments of the *Trb* locus and express intracellular (ic)TCR $\beta$ . They are selected by a process known as the  $\beta$ -selection checkpoint at which icTCR $\beta$ <sup>positive</sup> DN3b cells undergo a proliferative burst and have an increased metabolic state as shown by CD98 expression (3, 4). This dramatically expands the pool of thymocytes with successful *Trb* rearrangements, which can progress to the double-positive (DP) stage of development (2). During VDJ recombination, double-strand DNA breaks (DSBs) are formed by the RAG complex and activate the DNA damage response (DDR) pathway. These lead to activation of ataxia-telangiectasia–mutated (Atm), DNA-dependent kinase catalytic subunit, and Atm- and Rad3-related (Atr) (5, 6). A critical target of these kinases is histone variant H2AFX, which is phosphorylated (p-H2AFX) at the site of DNA damage (7). p-H2AFX then recruits other DDR factors to the break site and stabilizes cleaved DNA ends prior to joining (8–11). Atm and DNA-dependent kinase catalytic subunit are also responsible for the activation of the Chk1 and Chk2 protein kinases, which phosphorylate multiple downstream effectors, including Cdc25a and p53, leading to cell cycle arrest and DSB resolution/repair (12, 13). Remarkably, the activation of these pathways has been linked to the promotion of thymocyte differentiation (14, 15) as well as transformation.

The ZFP36 family of RNA-binding proteins (RBP) comprises three gene family members in humans and four in mice. These RBPs bind to A/U-rich elements (AREs) in the 3' untranslated region (UTR) of mRNA and promote RNA decay (16). As such, many mRNAs have been proposed as targets of ZFP36 family proteins, although few have been shown to be physiologically relevant (16). Constitutive knockout (KO) of *Zfp36* leads to viable animals that develop an autoimmune disease caused by the overexpression of the proinflammatory cytokine TNF (17–19), whereas *Zfp3611*- or *Zfp3612*-null mice die in utero or shortly after birth due to disorganized vasculature or anemia, respectively

<sup>\*</sup>MedImmune, Cambridge CB21 6GH, United Kingdom; <sup>†</sup>Department of Medicine, Medical Research Council-Laboratory of Molecular Biology, University of Cambridge, Cambridge CB2 0QH, United Kingdom; <sup>‡</sup>School of Life Science, Centre for Gene Regulation and Expression, University of Dundee, Dundee DD1 5EH, United Kingdom; and <sup>§</sup>Laboratory of Lymphocyte Signalling and Development, Babraham Institute, Cambridge CB22 3AT, United Kingdom

<sup>1</sup>K.U.V. and L.S.B. contributed equally to this work.

ORCIDs: 0000-0001-8712-5372 (K.U.V.); 0000-0002-9412-7066 (L.S.B.); 0000-0001-8780-0382 (A.G.); 0000-0002-3801-9896 (M.T.).

Received for publication May 18, 2016. Accepted for publication July 26, 2016.

This work was supported by the Biotechnology and Biological Sciences Research Council, a Medical Research Council centenary award and project grant from Bloodwise (A.G.), and the Federation of European Biochemical Societies (K.U.V.).

K.U.V. and L.S.B. did most of the experiments with A.G. contributing to specific experiments; H.A. did the bioinformatics analyses; M.T. supervised and provided guidance on the project; K.U.V., L.S.B., and M.T. wrote the manuscript.

The sequences presented in this article have been submitted to the Gene Expression Omnibus under accession number GSE79179.

Address correspondence and reprint requests to Dr. Martin Turner, Laboratory of Lymphocyte Signalling and Development, Babraham Institute, Babraham Research Campus, Cambridge CB22 3AT, U.K. E-mail address: martin.turner@babraham.ac.uk

The online version of this article contains supplemental material.

Abbreviations used in this article: ARE, A/U-rich element; Atm, ataxia-telangiectasia–mutated; Atr, ataxia-telangiectasia–mutated and Rad3-related; BM-HSC, bone marrow–derived hematopoietic stem cell; Cnd3, Cyclin D3; Ccne2, Cyclin E2; DCKO, double conditional knockout; DDR, DNA damage response; DN, double-negative; DP, double-positive; DSB, double-strand break; FDR, false discovery rate; GO, Gene Ontology; GSEA, gene set enrichment analysis; HSC, hematopoietic stem cell; ic, intracellular; iCLIP, individual nucleotide resolution cross-linking and immunoprecipitation; ILC2, type 2 innate lymphocyte cell; iSP, intermediate single-positive cell; KO, knockout; MFI, median fluorescence intensity; ncRNA, noncoding RNA; NP-40, Nonidet P-40; PdBU, phorbol ester phorbol-12,13-dibutyrate; RBP, RNA-binding protein; RNA-seq, RNA sequencing; RPKM, reads per kilobase of transcript per million mapped reads; T-ALL, T cell acute lymphoblastic leukemia; Tg, transgenic; UTR, untranslated region.

Copyright © 2016 by The American Association of Immunologists, Inc. 0022-1767/16/\$30.00

(20–22). During early B cell development, *Zfp3611/12* act redundantly to enforce quiescence and enable recombination of the Ig genes (23). Although the development of B cells lacking both *Zfp3611* and *Zfp3612* is impaired, these mice do not develop B cell malignancy. By contrast, the conditional deletion of both *Zfp3611* and *Zfp3612* (double conditional KO [DCKO]) in thymocytes results in the bypass of the  $\beta$ -selection checkpoint and development of T cell acute lymphoblastic leukemia (T-ALL) (24). These tumors are dependent on Notch1, for which expression is increased following the release of its mRNA from posttranscriptional repression by *Zfp3611/12*. However, the details of how the  $\beta$ -selection checkpoint is circumvented remain unknown. A better understanding of the spectrum of mRNAs bound by *Zfp3611/12* in thymocytes is necessary to elucidate the molecular mechanisms through which they regulate the development and proliferative properties of thymocytes.

In this report, we combine the detailed phenotypic analyses of early thymocytes from DCKO mice with genome-wide approaches to identify the molecular mechanisms regulated by the RBPs. We integrate RNA sequencing (RNA-seq) gene expression data with individual nucleotide resolution cross-linking and immunoprecipitation (iCLIP) (25) to identify RBP binding positions within their mRNA targets. Our results show that DN3 thymocytes lacking *Zfp3611/12* closely share gene expression profiles with postselection DN3b wild-type thymocytes, despite having reduced VDJ recombination of *Trbv* gene segments and being  $\text{iTCR}\beta$  negative. Furthermore, DCKO thymocytes have elevated expression of positive cell cycle regulators and show increased cycling and DDR pathway activation *in vivo*. Conversely, overexpression of a *GFPZFP36L1* transgene reduces cell cycle entry. Inhibition of the cell cycle in DCKO mice by treatment with a *Cdk4/6* inhibitor partially rescues  $\text{iTCR}\beta$  expression in DN3 thymocytes. Thus, *Zfp3611/12* limit the cell cycle in developing thymocytes and the persistence of DSBs in cycling cells.

## Materials and Methods

### Mouse strains

C57BL/6 mice were from The Jackson Laboratory and bred at the Babraham Institute. *Zfp3611<sup>fl/fl</sup>*, *Zfp3612<sup>fl/fl</sup>*, *CD2cre* DCKO mice were previously described (24). *GFPZFP36L1* transgenic (Tg) mice were generated by targeting the *ROSA26* locus using standard methods (23). For cell type-specific Cre expression, *CD2cre* [Tg(CD2-cre)4Kio] mice were used (26), and for assessing Myc expression, GFP-myc knockin mice (27) were crossed to DCKO mice. All animal procedures were approved by the Animal Welfare and Experimentation Committee of the Babraham Institute and the U.K. Home Office.

### Flow cytometry

Single-cell suspensions of thymocytes were preincubated with Fc-block (anti-mouse CD16/CD31, clone 2.4G2; BioXCell) in staining buffer (PBS, 2% FBS, and 2 mmol/l EDTA) for 10 min at 4°C and stained with surface Abs for 20 min at 4°C. For intracellular staining of CD3e and TCR $\beta$ , the BD Cytotfix/Cytoperm kit (BD Biosciences) was used. For detection of phosphoproteins (Akt, Erk, Zap70/Syk, Stat5, and H2afx) and Cyclin D3 (Ccn3)/Cyclin E2 (Ccn2), cells were fixed with BD Lyse/Fix Buffer (BD Biosciences) and permeabilized with BD Phosflow Perm Buffer III (BD Biosciences). Afterwards, surface and intracellular proteins were stained in staining buffer for 1 h at room temperature. For detection of phosphorylated ATM substrates, cells were fixed with 4% paraformaldehyde and permeabilized with 90% methanol. Fixable Viability Dye eFluor 780 or DAPI (0.1  $\mu\text{g/ml}$ ) was used for assessing cell viability. For activated caspases, the CaspGLOW pan caspases kit (BioVision) was used according to the manufacturer's instructions. Samples were acquired on an LSRFortessa (BD Biosciences) and analyzed with FlowJo software (Tree Star). Abs were purchased from the following companies: cyclin E2 (E142), Abcam; B220 (RA3-6B2), CD3e (2C11), CD4 (RM4-5), CD25 (PC61), CD25 (7D4), cyclin D3 (1/Cyclin D3), Kit (ACK45), Ly6G (RB6-8C5), NK1.1 (PK136), p-Akt (M89-61), p-Stat5 (Y694, BD-TL), p-Zap70/Syk

(17A/P-ZAP70), TCR $\gamma\delta$  (GL3), rat anti-mouse IgG2b (R9-91), and BrdU (3D4), all from BD Biosciences; CD4 (RM4-5), CD8 (53-6.7), CD25 (PC61), CD44 (IM7), CD98 (RL388), CD127 (A7R34), Kit (ACK2), NK1.1 (PK136), p-H2ax (2F3), Sca1 (E13-161.7), TCR $\beta$  (H57-597), Thy1.1 (OX-7), and streptavidin, all from BioLegend; ATM substrates p-(Ser/Thr) and p-Erk (D13.14.4E), from Cell Signaling Technology; B220/CD45R (RA3-6B2), CD4 (GK1.5), CD11b (M1/70), CD24 (30F1), Ly6G (RB6-8C5), and TCR $\gamma\delta$  (eBioGL3), from eBioscience; ST2 (DJ8), mBioproducts; donkey anti-rabbit IgG, from Jackson ImmunoResearch Laboratories; and goat anti-rabbit IgG, Molecular Probes.

### Gating strategies

Lineage-negative excludes CD4, CD8, CD11b, TCR $\gamma\delta$ , NK1.1, B220, and GR1. DN thymocytes are CD4<sup>-</sup>, CD8<sup>-</sup>, and DN1 (CD44<sup>+</sup>, CD25<sup>-</sup>), DN2 (CD44<sup>+</sup>, CD25<sup>+</sup>), DN3 (CD44<sup>-</sup>, CD25<sup>+</sup>), DN3a (CD44<sup>-</sup>, CD25<sup>+</sup>, CD98<sup>low</sup>), DN3b (CD44<sup>-</sup>, CD25<sup>intermediate</sup>, CD98<sup>+</sup>), and DN4 (CD44<sup>-</sup>, CD25<sup>-</sup>), except for Fig. 1E and 1F, in which DN2 is (Lineage-negative, CD44<sup>+</sup>, Kit<sup>high</sup>) and DN3 is (Lineage-negative, CD44<sup>low</sup>, Kit<sup>low</sup>, CD25<sup>+</sup>). Intermediate single-positive cells (iSP) are (CD8<sup>+</sup>, CD24<sup>high</sup>) and mature CD8 (CD8<sup>+</sup>, CD24<sup>-</sup>). DP (CD4<sup>+</sup>, CD8<sup>+</sup>) cells are divided into early (CD98<sup>+</sup>, CD71<sup>+</sup>) and late (CD98<sup>+</sup>, CD71<sup>-</sup>) DPs. Type 2 innate lymphocyte cells (ILC2) are gated as (Lineage-negative, Thy1.1<sup>+</sup>, Sca1<sup>high</sup>, ST2<sup>+</sup>).

### BrdU analysis

For cell cycle analysis, mice were injected i.p. with 1 mg BrdU (BD Biosciences) diluted in sterile PBS (200  $\mu\text{l}$  of a 5-mg/ml solution). After 2.5 h, thymocytes were surface stained and then fixed using BD Cytotfix/Cytoperm (BD Biosciences). Cells were treated with 30  $\mu\text{g}$  DNase I (provided with the BD BrdU kit; BD Biosciences) for 1 h at 37°C, then washed, and stained intracellularly for BrdU and  $\text{iTCR}\beta$  for 1 h at room temperature. Cells were resuspended in BD Perm/Wash (BD Biosciences) containing 1  $\mu\text{g/ml}$  DAPI.

### OP9, OP9-DL1, and OP-DL4 culture

A total of 10,000 sorted DN3a (lineage-negative, CD44<sup>-</sup>, CD25<sup>+</sup>, CD98<sup>low</sup>) or DN3b (lineage-negative, CD44<sup>-</sup>, CD25<sup>intermediate</sup>, CD98<sup>+</sup>) thymocytes from *GFPZFP36L1*; *CD2cre* mice were seeded onto OP9-DL1 in 96 wells, supplemented with 1 ng/ml IL-7, and differentiation into CD4/CD8 DP cells was followed up to 3 d. Lineage markers were: CD11b, CD4, CD8, CD19, TCR $\gamma\delta$ , GR1, and Ter<sup>119</sup>. Cell sorting was done using an FACSARIA (BD Biosciences).

Coculture of bone marrow-derived hematopoietic stem cells (BM-HSCs) was performed as in Holmes and Zúñiga-Pflücker (28). Briefly, Sca1-enriched HSCs were obtained by magnetic cell sorting of lineage-negative cells and Sca1 enrichment with kits from Miltenyi Biotec. A total of 40,000–75,000 HSCs were seeded per six wells onto OP9-DL4 or OP9 cells with 1 ng/ml IL-7 and 5 ng/ml Flt3L. Cells were passaged on days 7, 12, and 15 to 16 with Flt3L and, in some cases, IL-7 being withdrawn from day 12 to allow differentiation. There was no difference in the performance between OP9-DL1 and OP9-DL4 cells in our experiments.

### IL-7 response and TCR signaling

For measuring IL-7 response, 10 million thymocytes were rested for 2 h at 37°C, then stimulated with 25 ng/ml IL-7 for 5, 30, 60, and 120 min, and immediately fixed with prewarmed BD Lyse/Fix Buffer (BD Biosciences). For assessing TCR signaling, cells were rested as above and stimulated for 2, 5, and 10 min with 50 ng/ml phorbol ester phorbol-12,13-dibutyrate (PdBu). After fixation, cells were permeabilized and stained for phosphoproteins as described in *Flow cytometry*.

### RNA-seq

RNA was isolated from sorted *Zfp3611<sup>fl/fl</sup>*; *Zfp3612<sup>fl/fl</sup>* DN3a (Lineage-negative, CD44<sup>-</sup>, Kit<sup>low</sup>, CD25<sup>+</sup>, CD98<sup>low</sup>) and DN3b (Lineage-negative, CD44<sup>-</sup>, Kit<sup>low</sup>, CD25<sup>intermediate</sup>, CD98<sup>+</sup>) cells as well as *Zfp3611<sup>fl/fl</sup>*; *Zfp3612<sup>fl/fl</sup>*; *CD2cre* DN3 (Lineage-negative, CD44<sup>-</sup>, Kit<sup>low</sup>, CD25<sup>+</sup>) cells with the RNeasy Micro Kit (Qiagen). RNA-seq libraries were prepared from 20–200 ng RNA using the TruSeq Stranded Total RNA and rRNA Removal Mix-Gold from Illumina. Libraries were sequenced by HisEquation 2000 in 100-bp single-end reads. Sequencing data quality control was carried out with FastQC (<http://www.bioinformatics.babraham.ac.uk/projects/fastqc/>). The reads were trimmed from adapter sequences using Trim Galore then mapped using Tophat (version 2.0.12) (29) to the genome assembly GRCm38. Multiply mapping reads were discarded. Reads aligning to genes were counted using htseq-count

(30). DESeq2 (R/bioconductor package) was used for analysis of differentially expressed genes (31). Data were generated from four biological replicates. Genes regulated  $>1 \log_2$  fold change (2-fold up- or downregulated), and adjusted  $p$  values  $<0.01$  were considered as significantly regulated. Results tables from differential expression and pathway analyses can be obtained upon request.

### Immunoprecipitation and Western blotting

Lysates (without crosslinking) and beads were prepared as described in the iCLIP procedure. Immunoprecipitation was performed with 500  $\mu\text{g}$  protein as described in the iCLIP procedure. Immunoblotting was performed by standard procedures. A total of 50  $\mu\text{g}$  protein of crude lysate was loaded and 10% of the unbound fraction or IP, respectively. Abs for immunoblotting were: anti-BRF1/2 (Cell Signaling Technology), anti-GFP (clone B2; Santa Cruz Biotechnology), and anti-Tubulin (DM1A; Sigma-Aldrich).

### iCLIP

iCLIP experiments were performed similar to previously described (Refs. 23, 25). Briefly, cell lysates were prepared from total thymocytes from C57BL/6 or DCKO mice, which were irradiated with 300  $\text{mJ}/\text{cm}^2$  UV light and then lysed in lysis buffer (50  $\text{mmol}/\text{l}$  Tris HCL [pH 8], 100  $\text{mmol}/\text{l}$  NaCl, 1% Nonidet P-40 [NP-40], 0.5% deoxycholate, 0.1% SDS, 1:200 protease inhibitor mixture [Sigma-Aldrich], and 500  $\text{U}/\mu\text{l}$  RNasin [New England Biolabs]). A total of 2.5  $\text{mg}$  protein supernatant was used per sample. Rabbit anti-ZFP36L1 Ab (BRF1/2; Cell Signaling Technology) was conjugated to Protein A-Dynabeads (Invitrogen) overnight.

Samples were treated with TURBO DNase and RNase I for partial RNA digest, and Zfp3611/RNA complexes were precipitated using bead-coupled rabbit anti-ZFP36L1 Ab (BRF1/2; Cell Signaling Technology). Washes were performed in high-stringency salt buffers (first iCLIP: 50  $\text{mmol}/\text{l}$  Tris-HCl [pH 7.4], 1  $\text{mol}/\text{l}$  NaCl, 1  $\text{mmol}/\text{l}$  EDTA, 1% NP-40, 0.2% SDS, and 0.5% sodium deoxycholate; second iCLIP: 50  $\text{mmol}/\text{l}$  Tris-HCl [pH 7.4], 1  $\text{mol}/\text{l}$  NaCl, 1  $\text{mmol}/\text{l}$  EDTA, 1% NP-40, 0.4% SDS, and 0.5% sodium deoxycholate) and PNK buffer (20  $\text{mmol}/\text{l}$  Tris-HCl [pH 7.4], 10  $\text{mmol}/\text{l}$   $\text{MgCl}_2$ , and 0.2% Tween-20). The RNA was then dephosphorylated, ligated to an RNA adaptor (L34: P-AUAGAUCGGAAGAGCGGUUCAG-Puromycin), and radioactively labeled. The RNA complexes were resolved on a denaturing SDS-PAGE and transferred to a nitrocellulose membrane. RNA was extracted and reverse transcribed into cDNA libraries. The cDNA libraries were sequenced by MiSeq as a 150-bp single-end read or as a HiSeq2500 RapidRun 50-bp single-end read and mapped to the mm10 mouse genome. iCLIP data were generated from two biological replicates for C57BL/6 and one for DCKO thymocytes. C57BL/6 data were merged during iCOUNT analysis. Unless specified, only binding to 3' UTR was considered. The analysis was performed as described in (25). Highly significant ZFP36L1 binding sites were identified using the iCount pipeline, and a false discovery rate (FDR) was assigned to each crosslink site as previously described (32). We only considered ZFP36L1 crosslink sites with an FDR  $<0.05$  in our analysis. iCount was also used to determine the kmer content of the cross-link sites.

RCLIP primers for C57BL/6 sample 1, 2, and DCKO were: RCLIP A, 5'-phosphate-NNNNGTTAGATCGGAAGAGCGTCTGGATCCTGAACCGTCTC-3'; RCLIP B, 5'-phosphate-NNNNGCCAGATCGGAAGAGCGTCTGGATCCTGAACCGTCTC-3'; and RCLIP C, 5'-phosphate-NNNATCAGATCGGAAGAGCGTCTGGATCCTGAACCGTCTC-3'.

### Gene set enrichment analysis

Differentially expressed mouse transcripts identified using DESeq2 (adjusted  $p < 0.01$ ) and  $>1$  iCLIP hits in the 3'UTR (FDR  $<0.05$ ) were analyzed for enriched Gene Ontology (GO) biological processes using Topfun (33). An FDR cutoff of 0.05 was applied. DNA damage checkpoint (GO Database: 0000077) genes were obtained from the GO biological pathways database.

### Palbociclib in vivo experiment

Palbociclib (Selleck Chemicals) was dissolved in 50  $\text{mmol}/\text{l}$  sodium lactate (Sigma-Aldrich) and administered once to mice by oral gavage at a dose of 150  $\text{mg}/\text{kg}$ . Mice were culled and analyzed 1 d after palbociclib administration.

### Statistics

Except for data generated by high-throughput sequencing, in which statistical tests are described elsewhere, all statistical analyses were made using Prism software (GraphPad). The test used and sample sizes are indicated in the figure legends.

## Results

### *Thymocytes deficient in Zfp3611 and Zfp3612 are committed to the T cell lineage but fail $\beta$ -selection*

To investigate how the loss of *Zfp3611* and *Zfp3612* leads to a bypass of  $\beta$ -selection, we first performed detailed flow cytometry analysis of thymocytes from *Zfp3611<sup>fl/fl</sup>*, *Zfp3612<sup>fl/fl</sup>*, *CD2Cre* DCKO and Cre-negative *Zfp3611<sup>fl/fl</sup>*, *Zfp3612<sup>fl/fl</sup>* (control) mice. CD44 expression within the CD4- and CD8-DN population of the DCKO mice was increased (Fig. 1A) as well as surface expression of Sca1 (Fig. 1B, Supplemental Fig. 1A), a marker of the more immature developmental stages of thymocytes. ILC2s are characterized by expression of Sca1, CD44, and CD25 (34–36) and have been shown to originate from HSCs in culture (37). We therefore investigated the possibility that ILC2s are aberrantly populating the thymus of DCKO mice. Staining for ST2<sup>positive</sup>, Sca1<sup>high</sup> ILC2s showed that their percentage and number was significantly increased in the thymus of DCKO mice compared with control mice (Supplemental Fig. 1B, 1C). However, the absolute number of these cells was  $<10,000$ . An overlay of the ILC2 population with DN subsets based on CD44 and CD25 surface expression showed that ILC2s did not contribute to the aberrant CD44<sup>high</sup> cells seen in DCKO mice, as they were CD44<sup>high</sup> and CD25<sup>intermediate</sup> (Supplemental Fig. 1D, 1E). We next determined whether these cells were committed to the T cell lineage. Commitment is marked by low levels of Kit and the expression of intracellular CD3 $\epsilon$  [icCD3 $\epsilon$  (38)]. Within DCKO mice, the abnormal CD44<sup>high</sup> population expresses icCD3 $\epsilon$  (Fig. 1C) and therefore represents DN3-like committed thymocytes. They exhibit higher expression of icCD3 $\epsilon$  than control DN3–4 cells (Supplemental Fig. 1F), but fail to express icTCR $\beta$ . During development, DCKO thymocytes are not efficiently selected for icTCR $\beta$  expression until they become mature T cells (Fig. 1D) (24). As a consequence, the number of DP cells is decreased in the DCKO (Fig. 1E, Supplemental Fig. 3F). The percentage of DN1, DN2, or DN3 populations is not changed in the DCKO compared with control; however, the percentage of DN4 cells is reduced (Fig. 1F). Because total thymocyte numbers are reduced, the numbers of DN3 and DN4 cells are decreased in the DCKO thymus (Fig. 1G, 1H). These data demonstrate that DCKO thymocytes are committed to the T cell lineage, but development is retarded from the DN3 stage onwards. To assess the contribution of the previously published *Zfp3611/12* mRNA target *Notch1* (24) to the phenotype, we assessed differentiation of control and DCKO BM-HSCs in a coculture system either with Notch ligand (OP9-DL4) or without (OP9) (27). DCKO HSCs differentiated faster into DP cells on OP9-DL4 feeder cells compared with control HSCs and were also able to differentiate into DP cells in the absence of Notch ligand (Fig. 1I). We therefore employed high-throughput approaches to identify additional pathways affected by loss of *Zfp3611/12*.

### *iCLIP and RNA-seq identify molecular pathways in thymocytes regulated by Zfp3611 and Zfp3612*

Because *Zfp3611* and *Zfp3612* promote RNA decay, biologically relevant targets of the RBPs were expected to be more abundant in DCKO cells. We therefore performed RNA-seq to measure mRNA abundance. As pre- and postselected DCKO DN3 cells cannot be subdivided on the basis of CD98 or icTCR $\beta$  (Fig. 1D, Supplemental Fig. 1G), we compared DCKO DN3 cells with sorted DN3a and DN3b cells from control animals (Supplemental Fig. 1H). Cluster analysis showed that the DN3 cells from DCKO mice (DCKO-DN3) were more closely related to wild-type DN3b (Ctrl-DN3b) than to DN3a cells (Ctrl-DN3a), despite their lack of icTCR $\beta$

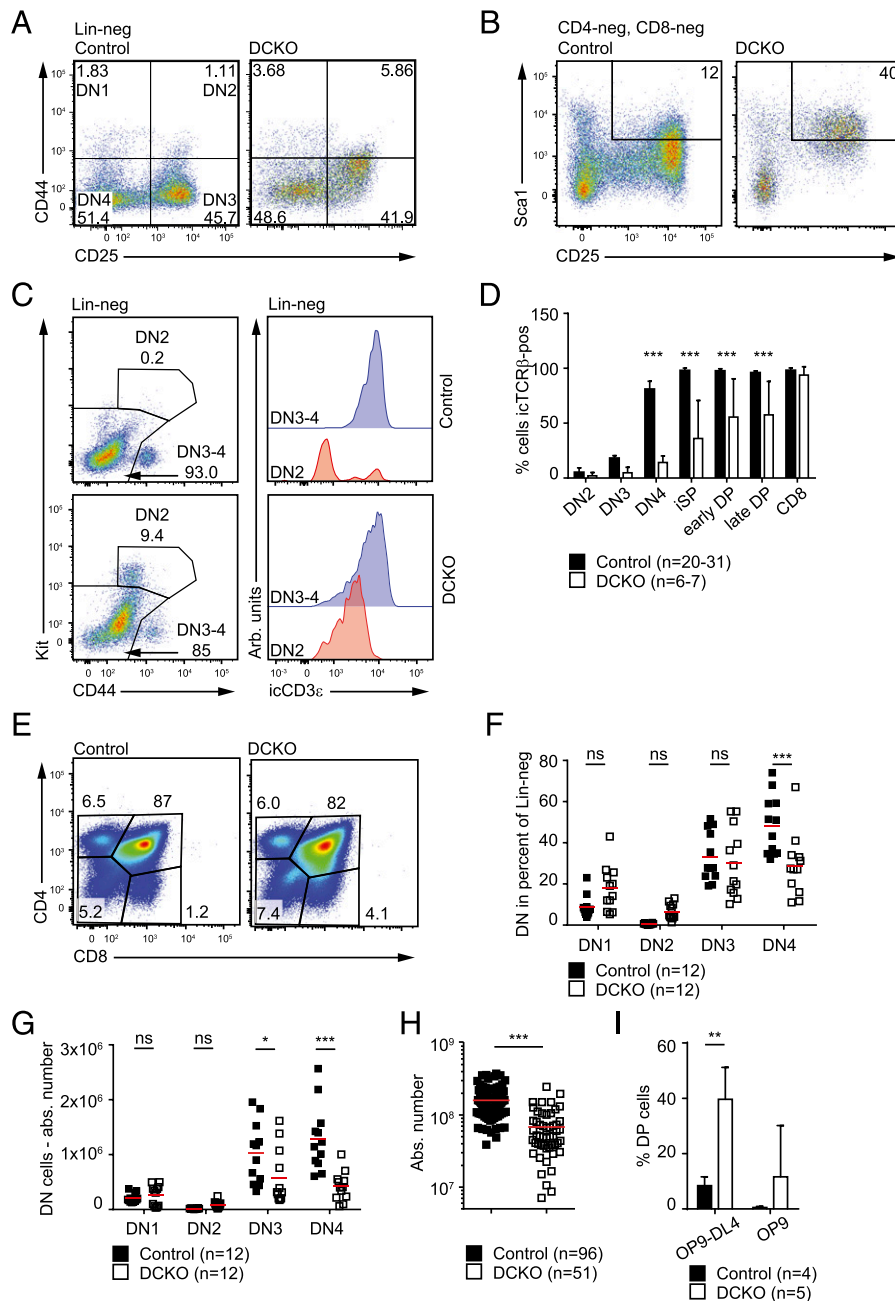
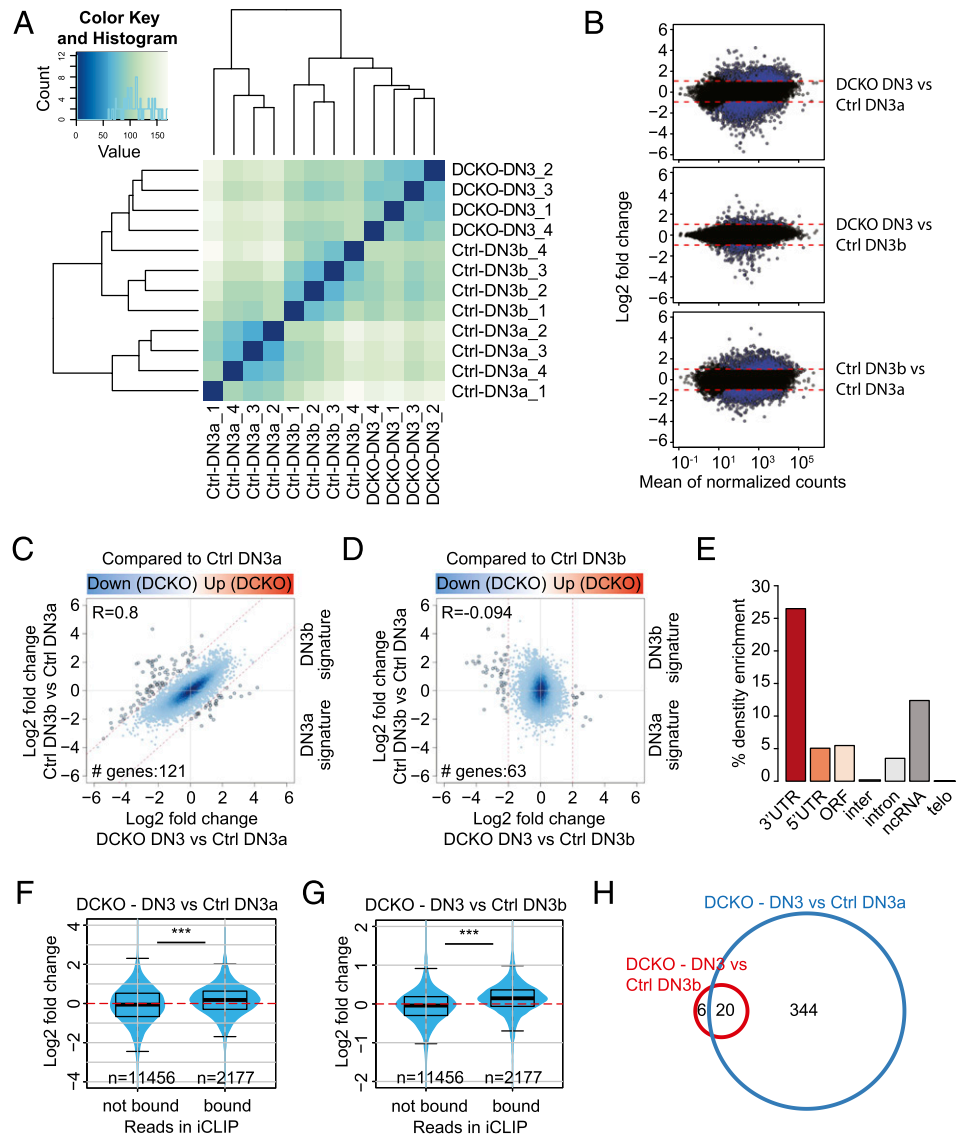


**FIGURE 1.** *Zfp36l1/2*-deficient thymocytes are committed to the T cell lineage but fail  $\beta$ -selection. **(A)** Representative FACS plots showing proportions of DN1, DN2, DN3, and DN4 thymocytes from control (*Zfp36l1/2*<sup>fl/fl</sup>) and *Zfp36l1/2*<sup>fl/fl</sup>; *CD2Cre* (DCKO) mice, gated on Lin<sup>-</sup> cells. Note that gating differs in this study from previous work (24), as we have identified that thymocytes previously gated as DN2 express icCD3e and therefore are committed to the T cell lineage. **(B)** Representative FACS plots showing proportions of Scat<sup>+</sup> cells from control and DCKO mice gated on CD4<sup>-</sup>, CD8<sup>-</sup> cells. **(C)** Representative FACS plots showing proportions of Lin<sup>-</sup>, DN2 (Kit<sup>high</sup>, CD44<sup>+</sup>), and DN3-4 (Kit<sup>low</sup>, CD44<sup>low</sup>) cells from control and DCKO mice (left panel) and icCD3e expression in an overlay of DN2 and DN3-4 cells (right panel). **(D)** Percentage of icTCR $\beta$ -positive cells from control and DCKO mice in DN2-4 as gated in (A) and iSP (CD8<sup>+</sup>, CD24<sup>+</sup>), early DP (CD4<sup>+</sup>, CD8<sup>+</sup>, CD98<sup>+</sup>, CD71<sup>+</sup>), late DP (CD4<sup>+</sup>, CD8<sup>+</sup>, CD98<sup>+</sup>, CD24<sup>-</sup>), and CD8 (CD8<sup>+</sup>, CD24<sup>-</sup>). Data depicted as mean + SD. **(E)** Representative FACS plot showing proportions of live CD4, CD8, DP, and DN cells from control and DCKO mice. **(F)** Percentages of DN1-4 cells from control and DCKO mice, gated on Lin<sup>-</sup> and: DN1 = CD44<sup>+</sup>, CD25<sup>-</sup>; DN2 = CD44<sup>+</sup>, Kit<sup>high</sup>; DN3 = CD44<sup>-</sup>, Kit<sup>int-low</sup>, CD25<sup>+</sup>; and DN4 = CD44<sup>-</sup>, CD25<sup>-</sup>. **(G)** Absolute numbers of DN1, DN2, DN3, and DN4 cells from control and DCKO mice as described in (F). **(H)** Total number of thymocytes from control or DCKO mice. **(I)** Percentage DP cells derived from BM progenitors of control and DCKO mice after 20 d of coculture on OP9 or OP9-DL4 cells. Data depicted as mean + SD. Lin panel = CD4, CD8, CD11b, TCR $\gamma\delta$ , NK1.1, B220, and GR1. Data are from several (D), 4 (F and G), >10 (H), and 2 pooled (I) independent experiments with numbers of mice indicated in the figure. Horizontal lines indicate mean, and statistical significances were calculated by two-way ANOVA with Sidak multiple-comparisons test (D, F, G, and I) or unpaired *t* test (H) (\**p* < 0.05, \*\**p* < 0.01, \*\*\**p* < 0.001).

(Fig. 2A). A total of 3044 genes in the DCKO were differentially expressed compared with control DN3a cells and 519 genes compared with control DN3b cells (Fig. 2B, Supplemental Table I). To study in more detail how similar DCKO DN3 cells

are to control cells, the DN3a and DN3b signature genes (genes differentially regulated between wild-type DN3a and DN3b cells (Fig. 2B, Supplemental Table I) were plotted against the genes that were differentially regulated in the DCKO DN3 cells compared

**FIGURE 2.** *Zfp3611/2* control mRNA targets that are involved in the cell cycle. **(A)** Cluster analysis of RNA-seq samples showing the distance between sorted DN3a (control [Ctrl]-DN3a) or DN3b (Ctrl-DN3b) cells from control mice (*Zfp3611/2*<sup>fl/fl</sup>) and DN3 cells from *Zfp3611/2*<sup>fl/fl</sup>; *CD2Cre* (DCKO) mice (DCKO-DN3) (for gating strategy, see Supplemental Fig. 1H). **(B)** MA plots of differentially expressed genes in RNA-seq of DCKO DN3 versus Ctrl-DN3a (top panel), DN3b (middle panel), and Ctrl-DN3b versus Ctrl-DN3a (bottom panel) cells. Log<sub>2</sub> fold change values of DCKO samples compared with the DN3a **(C)** or DN3b **(D)** control samples are plotted against the comparison of control DN3b and DN3a samples. **(E)** Density enrichment of iCLIP hits, normalized to gene feature length. The y-axis represents percentage of enrichment. Log<sub>2</sub> fold change of RNA-seq mRNA expression from DCKO cells compared with control DN3a **(F)** or DN3b **(G)** and split into mRNA bound or not bound based on iCLIP results. **(H)** Venn diagram depicting the number of differentially regulated pathways in GSEA of genes bound in the iCLIP and differentially regulated (log<sub>2</sub> fold change) in RNA-seq of DCKO cells compared with control DN3a or DN3b cells. RNA-seq data are from four biological replicates each and iCLIP data from two biological replicates. \*\*\**p* < 0.001.



with either the control DN3a (Fig. 2C, Supplemental Table I) or DN3b cells (Fig. 2D, Supplemental Table I). DCKO DN3 cells showed strong positive correlation with the signature of DN3b when compared with DN3a cells ( $R = 0.8$ ) and none when compared with DN3b cells ( $R = -0.094$ ). Strikingly, many DN3b genes missing in the DCKO were *Trbv* genes (~30%), consistent with absence of iTCR $\beta$  protein expression. Notably, we found that the *Trbv* genes were expressed at considerably lower levels compared with control DN3a cells. These findings suggest that DCKO cells have progressed in development without the formation of the pre-TCR.

To identify those RNAs directly bound by *Zfp3611* and *Zfp3612*, we applied high-resolution iCLIP to mouse thymocytes (25). To this end, we used an Ab (BRF1/2), which recognizes mouse *Zfp3611* strongly and *Zfp3612* weakly on Western blots, but is selective for mouse *Zfp3611* when used for immunoprecipitation (Supplemental Fig. 2A). To further validate Ab specificity, we compared immunoprecipitations from C57BL/6 and DCKO thymocytes after UV crosslinking. After immunoprecipitation and partial RNA digestion by RNase I, the samples were labeled with [<sup>32</sup>P]γ-ATP. As expected, the C57BL/6 samples showed a greater signal on the autoradiograph than the DCKO (Supplemental Fig. 2B). Although there was little material in the DCKO sample, a DCKO library was prepared and sequenced for quality control

purposes. BRF1/2 immunoprecipitations from C57BL/6 thymus showed that crosslinks are present to a high degree in introns and intergenic regions. This is consistent between data from two individual and merged biological replicates (Supplemental Fig. 2C). After normalizing to segment lengths of each genomic feature, density enrichment was greatest for binding to 3' UTRs as well as noncoding RNAs (ncRNAs) (Fig. 2E, Supplemental Fig. 2D). To verify specific binding, we sought to identify the presence of ARE binding motifs in 3' UTRs and ncRNAs. Bound sequences from the two C57BL/6 replicates were plotted against each other and showed that AREs were highly enriched above the mean in bound 3' UTRs but not in bound ncRNAs (Supplemental Fig. 2E, 2F). Moreover, this enrichment of ARE motifs was only present in gene features from C57BL/6 and not in DCKO samples (Supplemental Fig. 2G), indicating the specificity of the interaction between *Zfp3611* and AREs within 3' UTRs.

Combining iCLIP and RNA-seq datasets is a powerful approach to identify both the direct targets of the RBPs and the effects on the transcriptome caused by loss of *Zfp3611* and *Zfp3612*. We therefore compared RNA-seq data from DCKO DN3 to either DN3a or DN3b control samples, divided on whether the RNA was bound or unbound in the iCLIP (Fig. 2F, 2G). There was a positive correlation between mRNA with increased expression in DCKO DN3 cells and bound iCLIP-identified targets. Thus, in the absence of

*Zfp36l1* and *Zfp36l2*, direct targets show increased expression of their RNA.

Gene set enrichment analysis (GSEA) of transcripts bound by *Zfp36l1* in the iCLIP and differentially up- or downregulated compared with DN3a or DN3b cells identified 364 pathways that were changed in the DCKO DN3 cells compared with control DN3a and 26 pathways that were changed compared with DN3b (Fig. 2H). Twenty pathways are distinct from either comparison and include the cell cycle and RNA metabolic processes (Supplemental Table II). DCKO DN3 differ from control DN3b cells in VDJ recombination, dephosphorylation, and T cell-activation pathways (Supplemental Table II). Together, the data show that DCKO DN3 cell phenotype wild-type DN3b cells but differ in expression of genes that are part of the cell cycle and VDJ recombination pathways.

#### *Increased cell cycling in early DN thymocyte subsets from DCKO mice*

The strong enrichment for cell cycle mRNA targets in the GSEA of the DCKO DN3 transcriptome could reflect a direct role of *Zfp36l1* and *Zfp36l2* in cell cycle control. Therefore, we assessed the cycling properties of DN thymocytes by measuring BrdU incorporation into the DNA of dividing cells 2.5 h after administration. DCKO DN4 and iSP that are  $\text{icTCR}\beta^{\text{positive}}$  showed a decrease in the percentage of cells in S-phase (Fig. 3A, left panel). By contrast,  $\text{icTCR}\beta^{\text{negative}}$  DN2 and DN3 cells from DCKO mice show a significantly increased percentage of cells in S-phase (Fig. 3A, right panel). Strikingly, *Zfp36l1*- and *Zfp36l2*-deficient DN3 cells exhibit a >5-fold increase in cycling cells over control DN3 thymocytes, which undergo cell cycle arrest to enable V-DJ recombination (2). Flow cytometric analysis showed the proportions of DN1, DN2, and DN3 cells from DCKO thymi positive for the cell cycle regulators *Ccnd3* and *Ccne2* were elevated. Moreover, these cells contained more *Ccnd3* and *Ccne2* mRNA and protein (Fig. 3B–G). Representative histograms are shown in Supplemental Fig. 2H and 2I. Myc, another key component promoting cell cycle progression, is also increased at the protein level in DN2 and DN3 cells, as assessed by a GFPmyc knockin allele (27) crossed to the DCKO (Fig. 3H).

Consistent with the DN3a to DN3b transition being linked to mitogenesis, control thymocytes show increased expression of both *Ccnd3* and *Ccne2* mRNA at the DN3b stage when compared with DN3a (Fig. 3D, 3G). However, DN3 cells from DCKO mice show an even greater elevation of *Ccne2* mRNA (Fig. 3G). Both *Ccnd3* and *Ccne2* mRNA were bound by *Zfp36l1* in the iCLIP, indicating that they are direct targets in thymocytes (Supplemental Fig. 2J, 2K). Binding of *Zfp36l1/2* to an ARE in Cyclin E2 mRNA was further validated by luciferase assays (23). Myc mRNA was not differentially expressed in DCKO thymocytes (Supplemental Table I), but was bound in the iCLIP, which suggests that Myc may be controlled by *Zfp36l1/2* as well as the cell cycle. To corroborate these results, we investigated if the increased cell cycle properties of DCKO cells facilitate T cell differentiation. As sorted DN3 cells from DCKO mice rapidly died in culture (data not shown), we seeded BM-HSCs from control and DCKO mice onto OP9-DL4 cells (28). DCKO HSCs differentiated into DPs more rapidly than control cells (Fig. 3I, 3J). DCKO cells consistently expanded more until the first cell culture passage (day 7), but expanded similarly or less than control cells with following passages (day 12 onwards; Fig. 3K). This is consistent with the hypothesis that cell division is linked to differentiation in wild-type cells (39).

#### *The cell cycle is inhibited in GFPZFP36L1 Tg mice*

To examine if overexpression of ZFP36L1 can oppose the DCKO phenotype, we bred mice in which the endogenous *Rosa26* locus

had been engineered to express a cDNA encoding a *GFPZFP36L1* fusion protein in a Cre-dependent manner with *CD2Cre* mice. The expression of the fusion protein and endogenous *Zfp36l1* was then assessed by Western blotting (Supplemental Fig. 3A). *GFPZFP36L1* was of the predicted molecular size and mice homozygous for the modified *Rosa26* locus had higher fusion protein abundance than did heterozygotes. Endogenous *Zfp36l1* protein appeared to be expressed less in Tg animals than in controls, which we interpret to be due to suppression of the endogenous *Zfp36l1* transcript by the fusion protein through binding to its ARE (40). Flow cytometry for *GFPZFP36L1* indicated that this protein was expressed in each of the DN populations, but greatest expression was in DN3 thymocytes (Supplemental Fig. 3B, 3C). To establish whether the transgene was functional in DN thymocytes, we next measured the surface expression of Notch-1 on DN thymocytes from *GFPZFP36L1<sup>tg/tg</sup>; CD2Cre* mice as *Notch1* mRNA was previously found to be targeted by *Zfp36l1* and *Zfp36l2* (24). Reduced surface Notch-1 expression was found on DN2, DN3, and DN4 transgene-expressing thymocytes (Supplemental Fig. 3D), suggesting the *GFPZFP36L1* fusion protein was functional. Furthermore, introduction of the *GFPZFP36L1* transgene into the DCKO mice substantially restored the cellularity of the DP compartment (Supplemental Fig. 3E, 3F). Most notably, the percentage of  $\text{icTCR}\beta$ -expressing cells in the DN3 and DN4 subset was restored to wild-type levels in *GFPZFP36L1/DCKO* mice, showing that the *GFPZFP36L1* fusion protein can functionally complement loss of endogenous *Zfp36l1* (Supplemental Fig. 3G).

The *GFPZFP36L1* fusion protein affected thymic development as *GFPZFP36L1<sup>tg/tg</sup>; CD2Cre* mice had reduced numbers of total thymocytes (Supplemental Fig. 3H), but a significantly increased percentage and number of DN3b cells (Fig. 4A–C, Supplemental Fig. 3I). However, the proportion of these DN3b and of DN4 cells in S-phase was significantly less in *GFPZFP36L1<sup>tg/tg</sup>; CD2Cre* mice than in Cre-negative controls (Fig. 4D), indicating the fusion protein inhibits the proliferation of developing thymocytes. This was consistent with slower expansion (Fig. 4E) and differentiation (Fig. 4F) of sorted DN3a and DN3b cells from *GFPZFP36L1<sup>tg/tg</sup>; CD2Cre* mice in vitro. Expansion was not significantly changed, but the appearance of DPs was delayed following coculture of Tg BM-HSCs on OP9-DL4 cells (Fig. 4G–I). In these cultures, *GFPZFP36L1*-expressing cells appeared mostly at the DN3a stage (Fig. 4G–J). Taken together, these data suggest that the *GFPZFP36L1* limits proliferation and differentiation at the  $\beta$ -selection checkpoint.

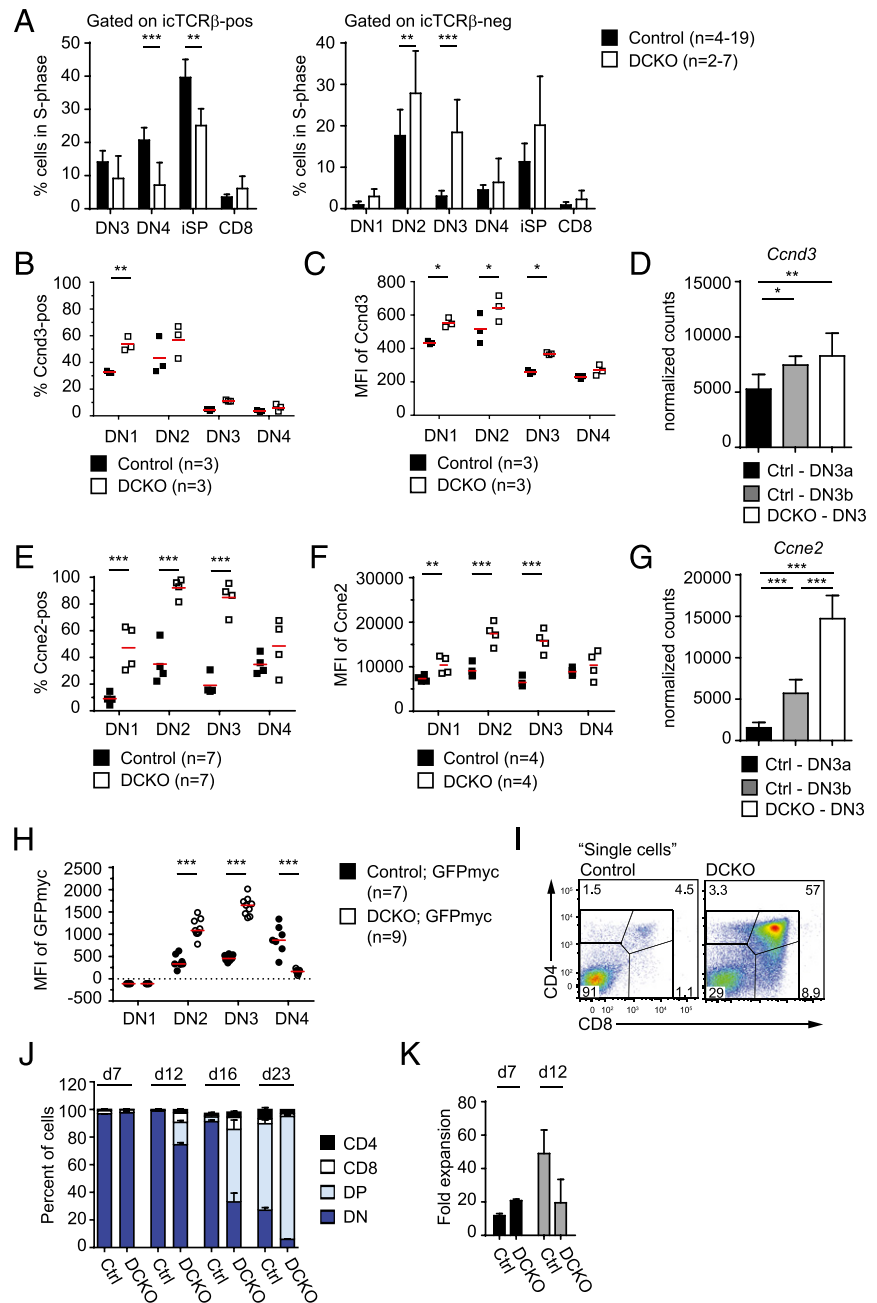
#### *Pharmacological inhibition of cell cycle progression partially rescues icTCR $\beta$ expression*

As cell cycle and VDJ recombination are linked in developing thymocytes (41), we tested whether  $\text{icTCR}\beta$  expression could be increased in DCKO mice by pharmacological inhibition of the cell cycle in vivo. To this end, G<sub>1</sub> to S progression was blocked with Palbociclib, a specific Cdk4/6 inhibitor by administering the drug to DCKO and control mice for 24 h. Palbociclib treatment reduced the percentage of cells in S-phase in DCKO DN3a slightly (Fig. 5A) but significantly diminished S-phase-positive DN3b cells from both DCKO and control animals (Fig. 5B). Treatment also increased  $\text{icTCR}\beta$  expression in DN3a cells and DN3b cells in both groups (Fig. 5C, 5D). However, this increase was not to wild-type DN3b levels of  $\text{icTCR}\beta$ ; thus, the rescue was incomplete. This suggests that inhibition of the cell cycle alone is insufficient to fully restore the  $\text{icTCR}\beta$ -positive DN3b population in DCKO mice.

#### *Lack of pre-TCR signaling in thymocytes of DCKO mice correlates with increased apoptosis*

Our observations are consistent with previously published work demonstrating a crucial but insufficient role of the cell cycle in

**FIGURE 3.** The cell cycle is increased in *Zfp3611/2<sup>fl/fl</sup>*; *CD2Cre* (DCKO) mice. **(A)** Percentage of BrdU<sup>+</sup> cells in S-phase (gated as in Fig. 1D with DN1 = Lin<sup>-</sup>, CD44<sup>+</sup>, CD25<sup>-</sup>) and split into iTCRβ<sup>+</sup> and iTCRβ<sup>-</sup> cells. Data are depicted as mean + SD and collated from 4–19 control (*Zfp3611/2<sup>fl/fl</sup>*) and 2–7 DCKO mice. **(B)** Percentage of *Ccnd3*-positive DN1–4 cells from control and DCKO mice. **(C)** MFI of *Ccnd3* as depicted in (B). **(D)** Normalized counts of *Ccnd3* mRNA in control DN3a (Ctrl-DN3a) or DN3b (Ctrl-DN3b) and DN3 cells from DCKO mice (DCKO-DN3). RNA-seq data were obtained from sorted thymocytes as described in Supplemental Fig. 1H. Data depicted as mean + SD of four biological replicates with statistical significances calculated by differential expression analysis (\**p* < 0.05, \*\**p* < 0.01). **(E)** Percentage of *Ccne2*-positive DN1–4 cells from control and DCKO mice. **(F)** MFI of *Ccne2* as depicted in (E). **(G)** Normalized counts of *Ccne2* mRNA as described in (D) (\*\**p* < 0.001). **(H)** MFI of GFPmyc in DN subsets from control; *GFPmyc* and DCKO;*GFPmyc* mice, which were crossed with *GFPmyc* reporter mice. Data are from two pooled experiments. **(I)** Representative FACS plots showing CD4/CD8 expression of BM-HSCs from control and DCKO mice after 16 d of coculture on OP9-DL4 cells. **(J)** Percentage of BM-HSCs from Ctrl and DCKO mice expressing CD4, CD8, or CD4/CD8 (DP) markers or no CD4/CD8 (DN) after 7, 12, 16, and 23 d of coculture on OP9-DL4 cells. **(K)** Fold expansion of BM-HSCs from control and DCKO mice after 7 and 12 d of coculture on OP9-DL4 cells in the presence of 1 ng/ml IL-7. Data are representative of 2 (B, C, E, and K), 3 (F), or 4 (I and J) independent experiments with 6 (B and E), 7 (C), 11 (F), and 10–11 (I and J) mice per genotype. Horizontal lines indicate mean and statistical significances were calculated by two-way ANOVA with Holm–Sidak multiple-comparisons test (\**p* < 0.05, \*\**p* < 0.01, \*\*\**p* < 0.001).



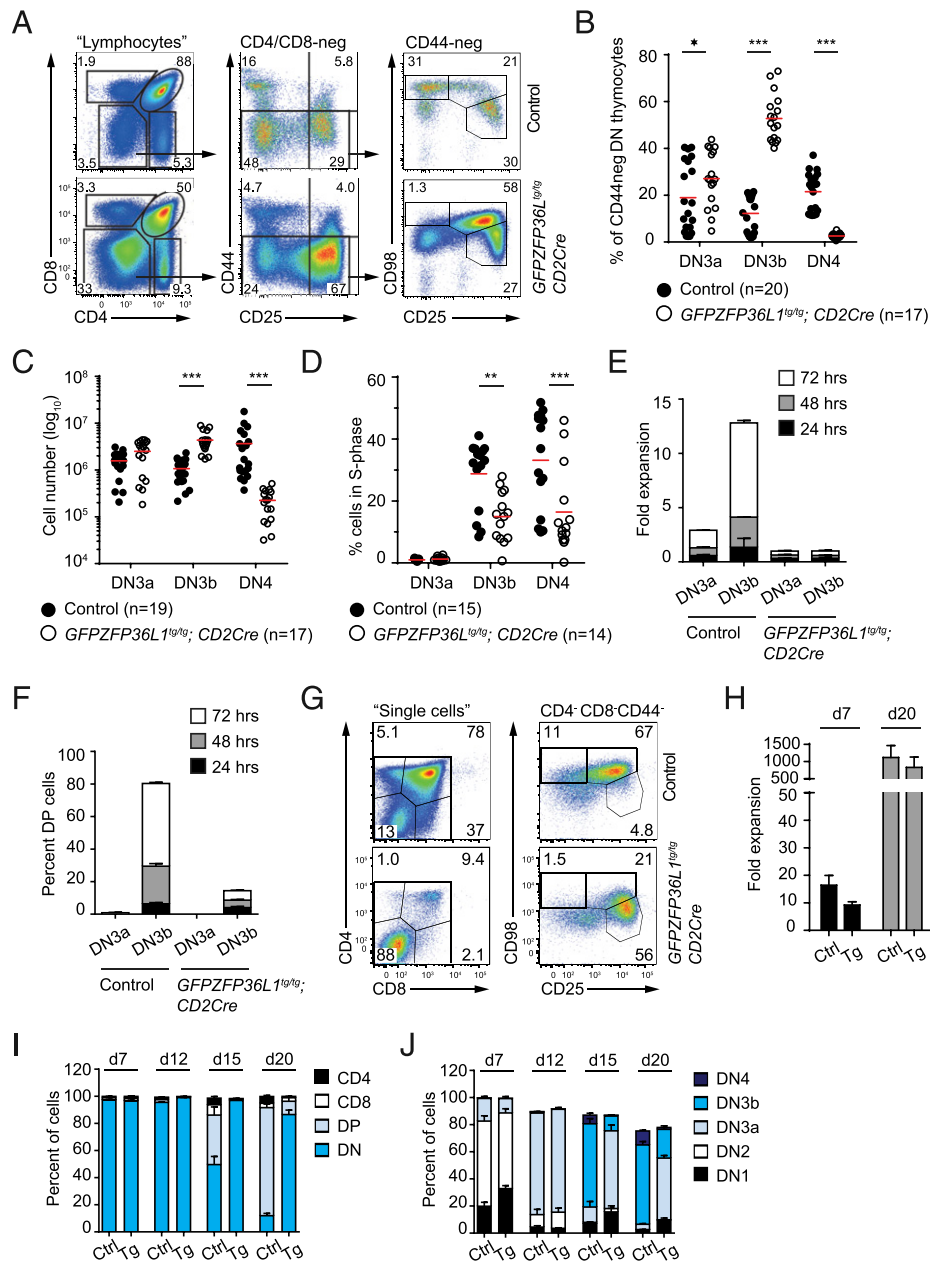
β-selection; overexpression of several genes promoting cell cycle progression could not override β-selection in the absence of pre-TCR signaling (39). These were *Ccnd3*, *Ccne1*, *Cdk2*, and *Cdk6*, of which all but *Ccne1* were detected as *Zfp3611* targets in our iCLIP. We therefore hypothesized that signaling events downstream of the pre-TCR could be activated by deregulation of direct *Zfp3611* or *Zfp3612* mRNA targets or through indirect-feedback mechanisms. To assess pre-TCR activity in DN subsets, we measured levels of Akt and Erk phosphorylation by phospho-flow cytometry under basal conditions as well as after PdBU stimulation of thymocytes from control or DCKO mice to assess feedback mechanisms. There was no evidence of elevated Akt and Erk activation (Fig. 5E).

IL-7 signaling is critical for thymocyte development. After transition from DN3a to DN3b, wild-type cells transiently up-regulate the IL-7R to receive survival signals (42). However, this upregulation could not be detected in the DN3b-like population of DCKO mice (Fig. 5F), likely reflecting the absence of the pre-TCR signal in the majority of these cells. In accordance with this

finding, IL-7-dependent STAT-5 phosphorylation is diminished in DN3 and DN4 cells from DCKO mice (Fig. 5G). Consistent with a lack of survival signal, we found increased apoptosis among late DN3 (CD25<sup>intermediate</sup>) and DN4 (CD25<sup>low</sup>) DCKO cells, as determined by the percentage of sub-G<sub>1</sub> cells (Fig. 5H). Increased total caspase activity was also evident in late DN3 cells from DCKO animals (Fig. 5I). We conclude that DCKO thymocytes die in part because of a failure to induce pre-TCR and IL-7R-dependent survival signals.

*Zfp3611* and *Zfp3612* limit the DNA damage response in thymocytes

As described above, one of the most striking observations in the RNA-seq data was the complete lack of *Trbv* transcripts in DCKO DN3 cells. We visualized D, J, and V gene expression by plotting their reads per kilobase of transcript per million mapped reads (RPKM) values derived by RNA-seq of control DN3a, DN3b, and DCKO DN3 cells (Fig. 6A–C). Although *Trbj* gene transcripts

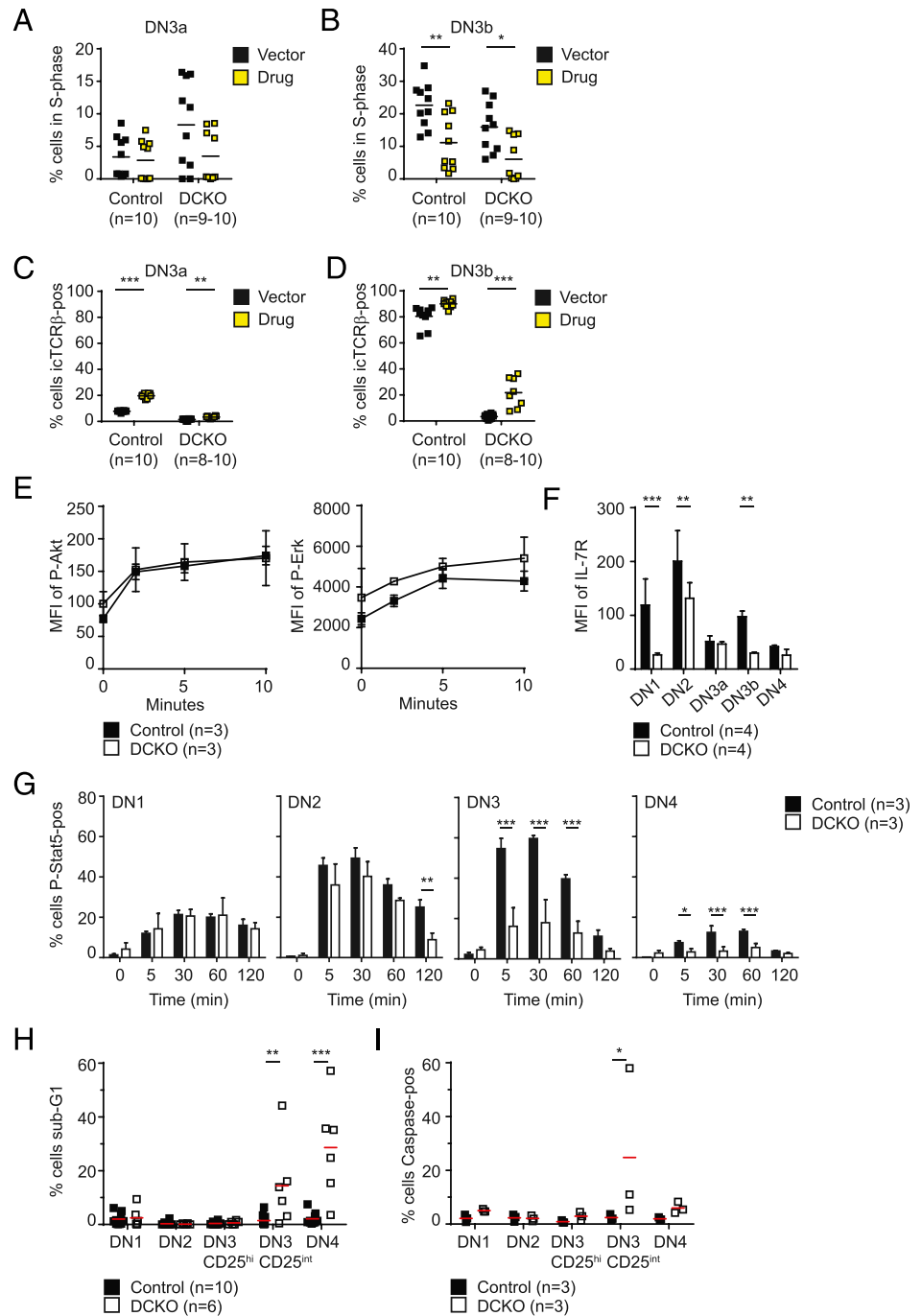


were readily detectable in DCKO DN3 cells, there was hardly any detectable *Trbv* transcript expression (Fig. 6B, 6C), suggesting a deficiency in V to DJ recombination.

Several groups have demonstrated that the block in VDJ recombination seen in *scid* mice could be overcome by DNA

damaging agents, which led to the development of thymic lymphomas (43–45). We therefore assessed the degree of DNA damage-related signaling in DN cells from DCKO mice by staining for phosphorylated H2afx, a marker typically associated with DNA DSBs (46). The percentage of p-H2afx<sup>positive</sup> DN3 cells

**FIGURE 5.** Lack of iCTCR $\beta$  signaling correlates with increased apoptosis and is only partially rescued by pharmacological inhibition of cell cycle progression. **(A)** Percentage of DN3a cells in S-phase (as gated on DAPI profile) from control (*Zfp3611/2<sup>fl/fl</sup>*) and *Zfp3611/2<sup>fl/fl</sup>; CD2Cre* (DCKO) mice, after 1 d of treatment with vector or palbociclib (drug). **(B)** Percentage of DN3b cells in S-phase as described in (A). **(C)** Percentage of DN3a cells positive for iCTCR $\beta$  as described in (A). **(D)** Percentage of DN3b cells positive for iCTCR $\beta$  as described in (A). **(E)** MFI of p-Akt and p-Erk in DN3 cells (CD44<sup>+</sup>, CD25<sup>+</sup>) from control (*Zfp3611/2<sup>fl/fl</sup>*) and *Zfp3611/2<sup>fl/fl</sup>; CD2Cre* (DCKO) mice after 0, 2, 5, and 10 min of PdBU stimulation. Depicted is the mean  $\pm$  SD. **(F)** MFI of IL-7R on DN subsets from control and DCKO mice. Depicted is the mean  $\pm$  SD. **(G)** Percentage p-Stat5-positive DN1–4 cells from control and DCKO mice after 0, 5, 30, 60, and 120 min of stimulation with IL-7. Depicted is the mean  $\pm$  SD. **(H)** Percentage of cells in sub-G<sub>1</sub> cell cycle phase of DN subsets from control and DCKO mice. Horizontal line represents the mean. **(I)** Percentage of caspase-positive cells in DN subsets as gated in (H) from control and DCKO mice. Horizontal line represents the mean. Data are representative of 3 [(E), p-Akt; (G)], 2 [(E), p-Erk], 4 (F), and 1 (I) independent experiments with 6–9 (E), 12–14 (F), 9 (G), and 3 (I) biological replicates per genotype. (A–D and H) Data are collated from two independent experiments with 8–10 (A–D) and 6–10 (H) mice as indicated in the figure. The horizontal line represents the mean with statistical significances calculated by two-way ANOVA with Sidak multiple-comparisons test (A–D, F, and G) or Holm–Sidak multiple-comparisons test (H and I) (\* $p < 0.05$ , \*\* $p < 0.01$ , \*\*\* $p < 0.001$ ).



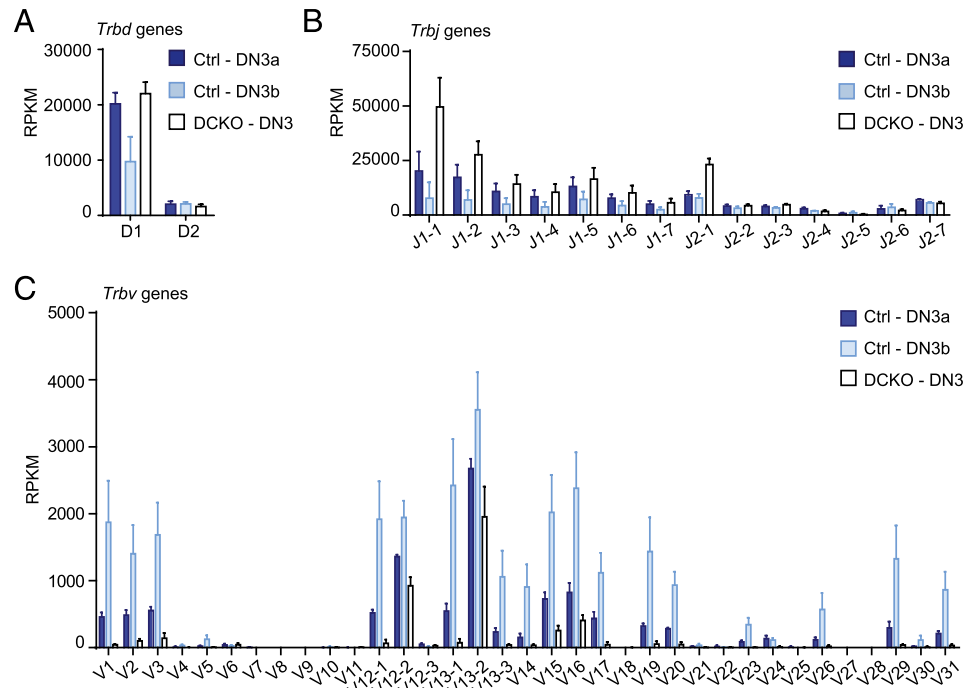
from DCKO mice was significantly increased compared with controls, as was the median fluorescence intensity (MFI) of p-H2afx staining (Fig. 7A–C). Furthermore, we found increased staining with an Ab detecting phosphorylated Atr/Atm substrates in DN1 and notably in DN3 cells from knockout mice (Fig. 7D, 7E). The MFIs of p-Chek1 and Mdm2, which are Atr/Atm substrates, were also significantly increased in DCKO DN3 cells (Fig. 7F–I). Furthermore, we found Mdm2 mRNA levels increased in DCKO DN3 cells (Fig. 7J) and the 3' UTR of Mdm2 was bound by Zfp3611 in the iCLIP (Fig. 7K), suggesting Mdm2 is a potential direct target of Zfp3611/2.

To confirm whether Zfp3611 and Zfp3612 may be directly regulating the DDR, we separated a list of DNA damage-related genes based on whether their transcripts were bound or not bound in the iCLIP and checked their expression in the RNA-seq dataset. As

expected, the expression of DNA damage-related transcripts was greatest in DCKO DN3 when compared with control DN3a cells, irrespective of whether the transcript was bound in the iCLIP (Fig. 7L). A comparison of DCKO DN3 cells with control DN3b cells revealed that the DNA damage-related transcripts bound in the iCLIP were significantly upregulated as opposed to unbound transcripts, which were unchanged (Fig. 7M). Given the similarity of DCKO DN3 cells to control DN3b cells (Fig. 2A), it is notable that only the DNA damage-related transcripts bound in the iCLIP were increased in DCKO mice.

Taken together, these data demonstrate that Zfp3611 and Zfp3612 directly control cell cycle transcripts and play an important role in controlling DNA damage-related transcripts connected to VDJ recombination to ensure the correct timing and progression of  $\beta$ -selection.

**FIGURE 6.** Lack of *Trbv* gene signature in DCKO mice. **(A)** RPKM values of *Trbd* genes in control (Ctrl; *Zfp36l1/12<sup>fl/fl</sup>*), DN3a (Ctrl-DN3a), DN3b (Ctrl-DN3b), and DN3 cells from *Zfp36l1/12<sup>fl/fl</sup>*; *CD2Cre* mice (DCKO-DN3). RNA-seq data were obtained from sorted thymocytes as described in Fig. 2A. Data are depicted as mean + SD of four biological replicates. **(B)** RPKM values of *Trbj* genes as described in (A). **(C)** RPKM values of *Trbv* genes as described in (A).



## Discussion

In this study, we demonstrated a novel posttranscriptional function of *Zfp36l1* and *Zfp36l2* in limiting the cell cycle and DDR signaling in developing thymocytes at the  $\beta$ -selection checkpoint. We propose that these RBPs limit several signaling pathways, of which the cell cycle and DNA damage pathway are driving forces for ensuring the proliferation and differentiation associated with  $\beta$ -selection. The previously identified regulation of *Notch1* mRNA by the RBPs is consistent with this model, as *Notch1* is an integral part of the mitogenic signal necessary for  $\beta$ -selection. Interestingly, overexpression of *ICN1* can promote differentiation of *Rag*-deficient thymocytes (47), and activating mutations in *ICN1* have been found in >50% of human T-ALL (48). However, *ICN1*-overexpressing cells that were deficient in the proximal pre-TCR signaling component *Lcp2* (*Slp76*) fail to develop into DPs. This suggests that *ICN1* requires the pre-TCR signaling machinery (47). Likewise, it was shown that *Notch3*-driven T-ALL was dependent on a functional pre-TCR (49). In this respect, it is possible that *Notch* signaling is not solely responsible for initiating the bypass of the  $\beta$ -selection checkpoint in DCKO mice, whereas it could still potentiate subsequent T-ALL development by a feed-forward loop (50). This is consistent with our data showing differentiation of DCKO HSCs in the absence of *Notch*-ligand and the lack of mRNA upregulation of *Notch*-target genes such as *Myc*, *Hes1*, and *Dtx1* in our RNA-seq dataset. Upregulation of *Notch1* (24) and *Myc* protein in the DCKO thymocytes may reflect an effect of the RBP on translation of these mRNAs, increased cell cycle feedback, lack of degradation by ubiquitinases such as *Fbxw7* (51–53), or a combination thereof. The identification of translational targets of the RBP and their distinction from targets regulated principally by RNA decay will require the generation and integration of additional datasets such as ribosomal footprinting (54).

Remarkably, even in the absence of productive VDJ rearrangements, activation of the DDR can promote the developmental progression of thymocytes. Irradiation induces differentiation and DP thymocyte development in both *Rag*-deficient and *scid* animals (43, 44, 45, 55). Although sensing of DSBs and cell cycle arrest is

important for enforcement of the  $\beta$ -selection checkpoint, proliferation is necessary but not sufficient for differentiation. Deletion of *Ccnd3* or inhibition of *Cdk4* and *Cdk6* can block thymocyte development both in vitro and in vivo. However, forced cell cycling cannot promote differentiation of *Rag*-deficient cells into DP thymocytes (39), indicating that the processes of proliferation and differentiation can be uncoupled.

Once the  $\beta$ -selection checkpoint is passed, *Ccnd3* cooperates with the DDR machinery and inhibits  $V_{\beta}$  transcription to ensure the allelic exclusion of *Trb* genes (41, 56). In B cells deficient for *Zfp36l1/12* (*Zfp36l1fl/fl*; *Zfp36l2fl/fl*; *Mb1cre*), loss of quiescence causes a failure to recombine and express *Ig $\mu$*  (23). In vivo cell cycle inhibition in mutant B cells rescues *Ig $\mu$*  VDJ recombination and the presence of pro- and pre-B cells containing excision circles. This is in contrast to our data showing only a partial rescue of *iTCR $\beta$*  expression in DCKO thymocytes upon cell cycle inhibition. We therefore propose that the feedback mechanisms between cell cycle and DDR are not functioning correctly in DCKO thymocytes. The gene list used to assess direct involvement of *Zfp36l1/12* targets in DDR comprises genes of DNA repair mechanisms as well as DDR downstream signaling, which either recruits factors to damaged DNA or induces stress pathways. The nature and contribution of individual targets is not yet clear. We suggest *Zfp36l1/12* control transcripts involved in DDR resolution and signaling or the generation of DSBs. Potential contributors could be *Rag1* and *Rag2*, which were identified as iCLIP targets and could play a role in the generation of breaks at the DN3 stage. It was also shown that overexpression of the *Zfp36l1/12* target *Mdm2* can inhibit DNA DSB repair (57). Although DNA repair could be delayed, we think it is likely to be functional, because mature T cells eventually express a TCR.

VDJ recombination is linked to apoptosis through the activation of *p53* by DNA DSBs. Although *p53* and *Atm* are essential for the containment of DSBs in noncycling cells (56), this process is finely balanced by a network of transcriptional and posttranscriptional mechanisms. In thymocytes undergoing VDJ recombination, the transcription factor *Miz-1*, for example, regulates the translation of *p53* via the ribosomal protein *Rpl22*, which associates with *p53*

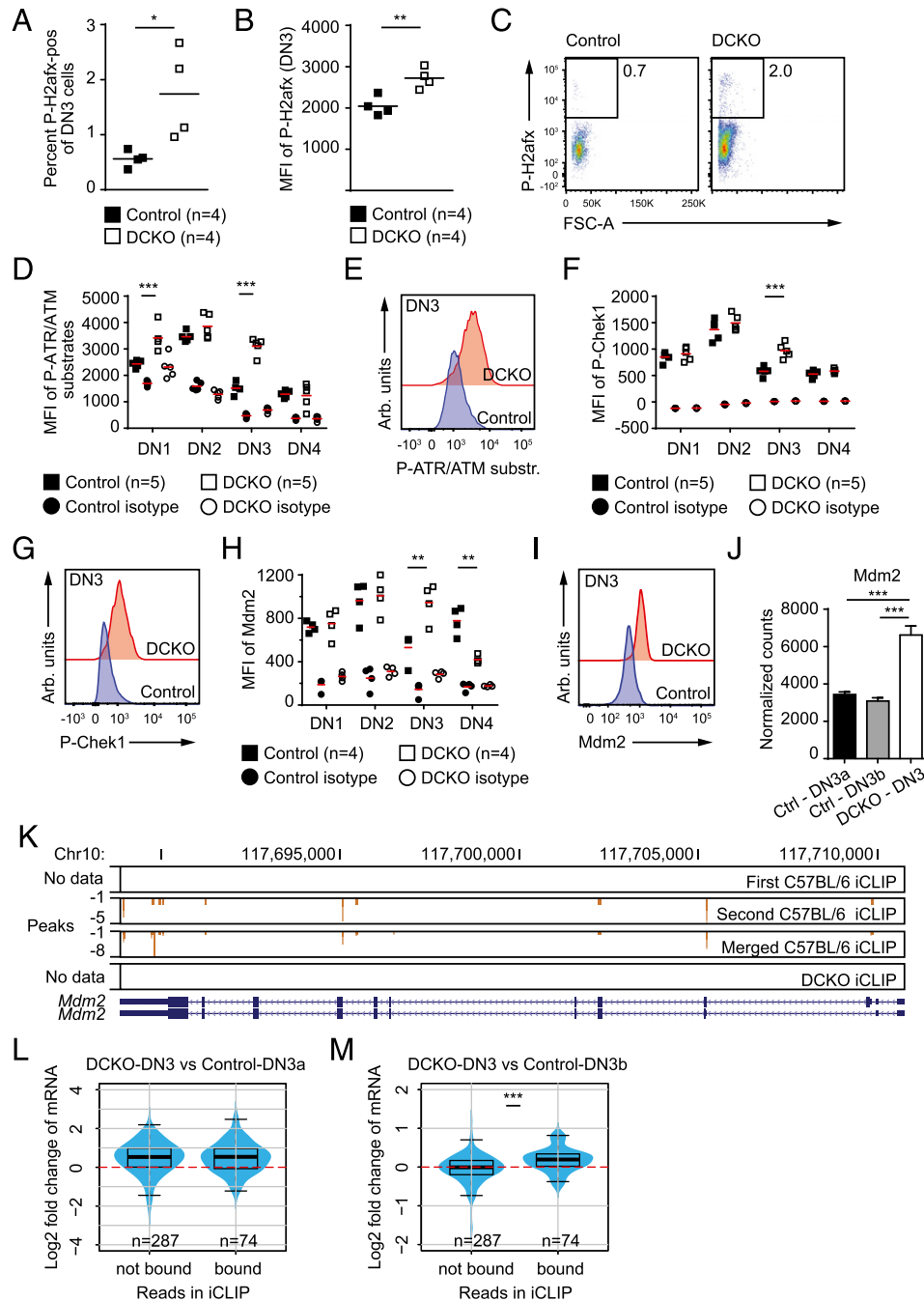


**FIGURE 7.** Zfp3611 and Zfp3612 limit the DDR in thymocytes. **(A)** Percentage of p-H2afx–positive DN3 cells of control and DCKO mice. Horizontal line represents the mean. **(B)** MFI of p-H2afx in DN3 cells as in **(A)**. **(C)** Representative FACS plots of p-H2afx expression in DN3 cells as in **(A)**. **(D)** MFI of p-ATR/ATM substrates in DN subsets from control and DCKO mice with respective isotype staining. Horizontal line represents the mean; significance calculated without including isotype staining. **(E)** Representative histogram overlay of p-ATR/ATM substrates in DN3 cells from control and DCKO mice. **(F)** MFI of p-Chk1 in DN subsets as in **(D)**. **(G)** Representative histogram overlay of p-Chk1 in DN3 cells from control and DCKO mice. **(H)** MFI of Mdm2 in DN subsets as in **(D)**. **(I)** Representative histogram overlay of Mdm2 in DN3 cells from control and DCKO mice. **(J)** Normalized counts of *Mdm2* mRNA in control DN3a (Ctrl-DN3a) or DN3b (Ctrl-DN3b) and DN3 cells from DCKO mice (DCKO-DN3). RNA-seq data were obtained from sorted thymocytes as described in Supplemental Fig. 1H. Data depicted as mean + SD of four biological replicates with statistical significances calculated by differential expression analysis ( $***p < 0.001$ ). **(K)** Genome tracks of Zfp3611 binding sites in the *Mdm2* gene with binding peaks of the individual and merged C57BL/6 and the DCKO iCLIP. Chromosomal location is indicated on the top, and genome features of *Mdm2* isoforms are shown on the bottom. The blue boxes depict exons connected by a line of arrows, which are introns. Narrow boxes indicate 5' or 3' UTRs. Log<sub>2</sub> fold change of mRNA expression of DNA damage genes from DCKO cells compared with control DN3a **(L)** or DN3b **(M)** and split into mRNA bound or not bound based on iCLIP data. Data are representative of 5 (**A–C**), 1 (**D–I**), and 2 (**L** and **M**) independent experiments with 16 (**A–C**), 5 (**D–G**), 4 (**H** and **I**), and 1 (**L** and **M**) biological replicates per genotype. Statistical significances were calculated by unpaired *t* test (**A** and **B**), two-way ANOVA with Sidak multiple-comparisons test (**D**, **F**, and **H**), or Wilcoxon test (**L** and **M**) ( $*p < 0.05$ ,  $**p < 0.01$ ,  $***p < 0.001$ ). Arb., arbitrary.

mRNA (58). We did not find a strong apoptosis gene signature in our RNA-seq or iCLIP data. Apoptosis-related genes such as *Bbc3* and *Bax* were not increased in DCKO DN3 cells; however, *Mdm2*

mRNA was bound in the iCLIP and elevated in DCKO DN3 cells. Consistent with this, *Mdm2* was identified by iCLIP as a target of the highly related Zfp36 RBP in a mouse macrophage cell line

(54). Mdm2 is a crucial inhibitor of p53 during lymphopoiesis (59), and p53 has been found downregulated in thymic tumors of DCKO mice (D. Hodson, A.A. Ferrando, and M. Turner, unpublished observations). Moreover, p53 deficiency can promote the development of DP thymocytes when pre-TCR signaling is compromised (60). Taken together, we suggest that increased Mdm2 could suppress p53-dependent cell death, arising in part from the lack of pre-TCR signaling, leading to DCKO cell survival in the presence of an increased DDR. Although we cannot fully rule out an involvement of Zfp36l1/2 in apoptosis pathways, we think it is more likely that the increased apoptosis we have shown in late DN thymocytes is a consequence of the lack of pre-TCR and IL-7-dependent survival signals. This is supported by the fact that the majority of  $\text{iTCR}\beta^{\text{negative}}$  cells die at the late DN3/DN4 stage of development.

Our data suggest that Zfp36l1/2 enforce the  $\beta$ -selection checkpoint and ensure its dependence on the pre-TCR signal. Firstly, the RBPs suppress cell cycle genes at the DN3a stage to allow time for productive VDJ recombination. In addition, they limit DDR gene expression to avoid bypass of the checkpoint due to the activation of this pathway. Upon the signaling of a productively rearranged pre-TCR, we speculate that Zfp36l1/2 function is suppressed by an as-yet-unknown mechanism relieving inhibition of target transcripts that promote cell cycle progression and allowing differentiation into mature T cells. Part of this response may be related to cessation of IL-7R signal transduction, which we showed to be dependent on Zfp36l1/2. IL-7 signaling inhibits expression of key transcription factors required for progression to and survival of the DP stage of thymocyte development (61). These include T cell factor 1, lymphoid enhancer-binding factor-1, and retinoic acid-related orphan receptor  $\gamma$ t. Moreover, IL-7 coordinates proliferation and rearrangement of TCR genes; thus, the phenotype may in part be influenced by altered IL-7 signaling (62). Exactly how the RBPs regulate IL-7 signaling is not known and could be the subject of future studies.

At the  $\beta$ -selection checkpoint, the timing of proliferation and VDJ recombination is crucial to avoid sustained chromosomal damage. DN3b cells must not be allowed to proliferate until productive VDJ recombination and the cessation of recombinase and DDR activity. Because transcription is a relatively slow process, the regulation of mRNA stability by RBPs such as Zfp36l1/2 can add dynamic flexibility to gene expression programs. Coupled with control of protein turnover, this form of control allows gene expression to be regulated in a fast and effective way so that DN3b cells can burst into proliferation upon a positive pre-TCR signal.

## Acknowledgments

We thank Vigo Heissmeyer, Manuel D. Díaz-Muñoz, and Dan Hodson for advice and comments on the manuscript; James Di Santo for OP9 DL4 cells; Manuel D. Díaz-Muñoz, Alexander Saveliev, Ram Venigalla, and Elisa Monzón-Casanova for technical advice; Sarah Bell, Kristina Tabbada, Arthur Davis, and Kirsty Bates for expert technical assistance; Simon Andrews, Jernej Ule, Igor Ruiz de los Mozos, and Tomaž Curk for help with iCLIP; and Michaela Frye for providing GFPmyc mice.

## Disclosures

The authors have no financial conflicts of interest.

## References

- Godfrey, D. I., J. Kennedy, T. Suda, and A. Zlotnik. 1993. A developmental pathway involving four phenotypically and functionally distinct subsets of CD3-CD4-CD8- triple-negative adult mouse thymocytes defined by CD44 and CD25 expression. *J. Immunol.* 150: 4244–4252.
- Rothenberg, E. V., J. E. Moore, and M. A. Yui. 2008. Launching the T-cell-lineage developmental programme. *Nat. Rev. Immunol.* 8: 9–21.
- Janas, M. L., and M. Turner. 2010. Stromal cell-derived factor 1 $\alpha$  and CXCR4: newly defined requirements for efficient thymic  $\beta$ -selection. *Trends Immunol.* 31: 370–376.
- Taghon, T., M. A. Yui, R. Pant, R. A. Diamond, and E. V. Rothenberg. 2006. Developmental and molecular characterization of emerging  $\beta$ - and gammadelta-selected pre-T cells in the adult mouse thymus. *Immunity* 24: 53–64.
- Ciccia, A., and S. J. Elledge. 2010. The DNA damage response: making it safe to play with knives. *Mol. Cell* 40: 179–204.
- Shiloh, Y. 2003. ATM: ready, set, go. *Cell Cycle* 2: 116–117.
- Rogakou, E. P., D. R. Pilch, A. H. Orr, V. S. Ivanova, and W. M. Bonner. 1998. DNA double-stranded breaks induce histone H2AX phosphorylation on serine 139. *J. Biol. Chem.* 273: 5858–5868.
- Celeste, A., O. Fernandez-Capetillo, M. J. Kruhlak, D. R. Pilch, D. W. Staudt, A. Lee, R. F. Bonner, W. M. Bonner, and A. Nussenzweig. 2003. Histone H2AX phosphorylation is dispensable for the initial recognition of DNA breaks. *Nat. Cell Biol.* 5: 675–679.
- Chen, H. T., A. Bhandoola, M. J. Difilippantonio, J. Zhu, M. J. Brown, X. Tai, E. P. Rogakou, T. M. Brotz, W. M. Bonner, T. Ried, and A. Nussenzweig. 2000. Response to RAG-mediated VDJ cleavage by NBS1 and gamma-H2AX. *Science* 290: 1962–1965.
- Fernandez-Capetillo, O., A. Lee, M. Nussenzweig, and A. Nussenzweig. 2004. H2AX: the histone guardian of the genome. *DNA Repair (Amst.)* 3: 959–967.
- Yin, B., V. Savic, M. M. Juntilla, A. L. Bredemeyer, K. S. Yang-Iott, B. A. Helmink, G. A. Koretzky, B. P. Sleckman, and C. H. Bassing. 2009. Histone H2AX stabilizes broken DNA strands to suppress chromosome breaks and translocations during V (DJ) recombination. *J. Exp. Med.* 206: 2625–2639.
- Dozier, C., M. Bonyadi, L. Baricault, L. Tonasso, and J.-M. Darbon. 2004. Regulation of Chk2 phosphorylation by interaction with protein phosphatase 2A via its B' regulatory subunit. *Biol. Cell* 96: 509–517.
- Helmink, B. A., and B. P. Sleckman. 2012. The response to and repair of RAG-mediated DNA double-strand breaks. *Annu. Rev. Immunol.* 30: 175–202.
- Yin, B., B.-S. Lee, K. S. Yang-Iott, B. P. Sleckman, and C. H. Bassing. 2012. Redundant and nonredundant functions of ATM and H2AX in  $\alpha\beta$  T-lineage lymphocytes. *J. Immunol.* 189: 1372–1379.
- Wang, C., M. A. Bogue, A. P. Nguyen, and D. B. Roth. 1999. Irradiation-induced rescue of thymocyte differentiation and V(D)J recombination in mice lacking the catalytic subunit of DNA-dependent protein kinase. *J. Immunol.* 163: 6065–6071.
- Brooks, S. A., and P. J. Blackshear. 2013. Tristetraprolin (TTP): interactions with mRNA and proteins, and current thoughts on mechanisms of action. *Biochim. Biophys. Acta* 1829: 666–679.
- Dang, C. V. 1999. c-Myc target genes involved in cell growth, apoptosis, and metabolism. *Mol. Cell Biol.* 19: 1–11.
- Taylor, G. A., E. Carballo, D. M. Lee, W. S. Lai, M. J. Thompson, D. D. Patel, D. I. Schenkman, G. S. Gilkeson, H. E. Broxmeyer, B. F. Haynes, and P. J. Blackshear. 1996. A pathogenetic role for TNF alpha in the syndrome of cachexia, arthritis, and autoimmunity resulting from tristetraprolin (TTP) deficiency. *Immunity* 4: 445–454.
- Lai, W. S., E. Carballo, J. R. Strum, E. A. Kennington, R. S. Phillips, and P. J. Blackshear. 1999. Evidence that tristetraprolin binds to AU-rich elements and promotes the deadenylation and destabilization of tumor necrosis factor alpha mRNA. *Mol. Cell Biol.* 19: 4311–4323.
- Bell, S. E., M. J. Sanchez, O. Spasic-Boskovic, T. Santalucia, L. Gambardella, G. J. Burton, J. J. Murphy, J. D. Norton, A. R. Clark, and M. Turner. 2006. The RNA binding protein Zfp36l1 is required for normal vascularisation and post-transcriptionally regulates VEGF expression. *Dev. Dyn.* 235: 3144–3155.
- Stumpo, D. J., H. E. Broxmeyer, T. Ward, S. Cooper, G. Hangoc, Y. J. Chung, W. C. Shelley, E. K. Richfield, M. K. Ray, M. C. Yoder, et al. 2009. Targeted disruption of Zfp36l2, encoding a CCCH tandem zinc finger RNA-binding protein, results in defective hematopoiesis. *Blood* 114: 2401–2410.
- Zhang, L., L. Prak, V. Rayon-Estrada, P. Thiru, J. Flygare, B. Lim, and H. F. Lodish. 2013. ZFP36L2 is required for self-renewal of early burst-forming unit erythroid progenitors. *Nature* 499: 92–96.
- Galloway, A., A. Saveliev, S. Łukasiak, D. J. Hodson, D. Bolland, K. Balmanno, H. Ahlfors, E. Monzon-Casanova, S. C. Mannurita, L. S. Bell, et al. 2016. RNA-binding proteins ZFP36L1 and ZFP36L2 promote cell quiescence. *Science* 352: 453–459.
- Hodson, D. J., M. L. Janas, A. Galloway, S. E. Bell, S. Andrews, C. M. Li, R. Pannell, C. W. Siebel, H. R. MacDonald, K. De Keersmaecker, et al. 2010. Deletion of the RNA-binding proteins ZFP36L1 and ZFP36L2 leads to perturbed thymic development and T lymphoblastic leukemia. *Nat. Immunol.* 11: 717–724.
- König, J., K. Zarnack, G. Rot, T. Curk, M. Kayikci, B. Zupan, D. J. Turner, N. M. Luscombe, and J. Ule. 2010. iCLIP reveals the function of hnRNP particles in splicing at individual nucleotide resolution. *Nat. Struct. Mol. Biol.* 17: 909–915.
- de Boer, J., A. Williams, G. Skavdis, N. Harker, M. Coles, M. Tolaini, T. Norton, K. Williams, K. Roderick, A. J. Potocnik, and D. Kioussis. 2003. Transgenic mice with hematopoietic and lymphoid specific expression of Cre. *Eur. J. Immunol.* 33: 314–325.
- Huang, C.-Y., A. L. Bredemeyer, L. M. Walker, C. H. Bassing, and B. P. Sleckman. 2008. Dynamic regulation of c-Myc proto-oncogene expression during lymphocyte development revealed by a GFP-c-Myc knock-in mouse. *Eur. J. Immunol.* 38: 342–349.
- Holmes, R., and J. C. Zúñiga-Pflücker. 2009. The OP9-DL1 system: generation of T-lymphocytes from embryonic or hematopoietic stem cells in vitro. *Cold Spring Harb. Protoc.* 2009: pdb.prot5156.
- Kim, D., G. Perrea, C. Trapnell, H. Pimentel, R. Kelley, and S. L. Salzberg. 2013. TopHat2: accurate alignment of transcriptomes in the presence of insertions, deletions and gene fusions. *Genome Biol.* 14: R36.

30. Anders, S., P. T. Pyl, and W. Huber. 2015. HTSeq - a python framework to work with high-throughput sequencing data. *Bioinformatics* 31: 166–169.
31. Love, M. L., W. Huber, and S. Anders. 2014. Moderated estimation of fold change and dispersion for RNA-seq data with DESeq2. *Genome Biol.* 15: 550.
32. Yeo, G. W., N. G. Coufal, T. Y. Liang, G. E. Peng, X.-D. Fu, and F. H. Gage. 2009. An RNA code for the FOX2 splicing regulator revealed by mapping RNA-protein interactions in stem cells. *Nat. Struct. Mol. Biol.* 16: 130–137.
33. Chen, J., E. E. Bardes, B. J. Aronow, and A. G. Jegga. 2009. ToppGene Suite for gene list enrichment analysis and candidate gene prioritization. *Nucleic Acids Res.* 37: W305–W311.
34. Sonnenberg, G. F., J. Mjösberg, H. Spits, and D. Artis. 2013. SnapShot: innate lymphoid cells. *Immunity* 39: 622–622.e1.
35. Spits, H., and J. P. Di Santo. 2011. The expanding family of innate lymphoid cells: regulators and effectors of immunity and tissue remodeling. *Nat. Immunol.* 12: 21–27.
36. Walker, J. A., J. L. Barlow, and A. N. J. McKenzie. 2013. Innate lymphoid cells—how did we miss them? *Nat. Rev. Immunol.* 13: 75–87.
37. Wong, S. H., J. A. Walker, H. E. Jolin, L. F. Drynan, E. Hams, A. Camelo, J. L. Barlow, D. R. Neill, V. Panova, U. Koch, et al. 2012. Transcription factor ROR $\alpha$  is critical for nuocyte development. *Nat. Immunol.* 13: 229–236.
38. Wilson, A., M. Capone, and H. R. MacDonald. 1999. Unexpectedly late expression of intracellular CD3 $\epsilon$  and TCR gammadelta proteins during adult thymus development. *Int. Immunol.* 11: 1641–1650.
39. Kreslavsky, T., M. Gleimer, M. Miyazaki, Y. Choi, E. Gagnon, C. Murre, P. Sicinski, and H. von Boehmer. 2012.  $\beta$ -Selection-induced proliferation is required for  $\alpha\beta$  T cell differentiation. *Immunity* 37: 840–853.
40. Stoeklin, G., S. A. Tenenbaum, T. Mayo, S. V. Chittur, A. D. George, T. E. Baroni, P. J. Blackshear, and P. Anderson. 2008. Genome-wide analysis identifies interleukin-10 mRNA as target of tristetraprolin. *J. Biol. Chem.* 283: 11689–11699.
41. Steinel, N. C., M. R. Fisher, K. S. Yang-Iott, and C. H. Bassing. 2014. The ataxia telangiectasia mutated and cyclin D3 proteins cooperate to help enforce TCR $\beta$  and IgH allelic exclusion. *J. Immunol.* 193: 2881–2890.
42. Trigueros, C., K. Hozumi, B. Silva-Santos, L. Bruno, A. C. Hayday, M. J. Owen, and D. J. Pennington. 2003. Pre-TCR signaling regulates IL-7 receptor  $\alpha$  expression promoting thymocyte survival at the transition from the double-negative to double-positive stage. *Eur. J. Immunol.* 33: 1968–1977.
43. Danska, J. S., F. Pflumio, C. J. Williams, O. Huner, J. E. Dick, and C. J. Guidos. 1994. Rescue of T cell-specific V(D)J recombination in SCID mice by DNA-damaging agents. *Science* 266: 450–455.
44. Guidos, C. J., C. J. Williams, G. E. Wu, C. J. Paige, and J. S. Danska. 1995. Development of CD4+CD8+ thymocytes in RAG-deficient mice through a T cell receptor  $\beta$  chain-independent pathway. *J. Exp. Med.* 181: 1187–1195.
45. Zúñiga-Pflücker, J. C., D. Jiang, P. L. Schwartzberg, and M. J. Lenardo. 1994. Sublethal gamma-radiation induces differentiation of CD4/CD8- into CD4+/CD8+ thymocytes without T cell receptor beta rearrangement in recombinationase activation gene 2<sup>-/-</sup> mice. *J. Exp. Med.* 180: 1517–1521.
46. Kuo, L. J., and L.-X. Yang. 2008.  $\gamma$ -H2AX - a novel biomarker for DNA double-strand breaks. *In Vivo* 22: 305–309.
47. Michie, A. M., A. C. Chan, M. Ciofani, M. Carleton, J. M. Lefebvre, Y. He, D. M. Allman, D. L. Wiest, J. C. Zúñiga-Pflücker, and D. J. Izon. 2007. Constitutive Notch signalling promotes CD4 CD8 thymocyte differentiation in the absence of the pre-TCR complex, by mimicking pre-TCR signals. *Int. Immunol.* 19: 1421–1430.
48. Weng, A. P., A. A. Ferrando, W. Lee, J. P. Morris, IV, L. B. Silverman, C. Sanchez-Irizarry, S. C. Blacklow, A. T. Look, and J. C. Aster. 2004. Activating mutations of NOTCH1 in human T cell acute lymphoblastic leukemia. *Science* 306: 269–271.
49. Bellavia, D., A. F. Campese, S. Checquolo, A. Balestri, A. Biondi, G. Cazzaniga, U. Lendahl, H. J. Fehling, A. C. Hayday, L. Frati, et al. 2002. Combined expression of pTalpha and Notch3 in T cell leukemia identifies the requirement of preTCR for leukemogenesis. *Proc. Natl. Acad. Sci. USA* 99: 3788–3793.
50. Palomero, T., W. K. Lim, D. T. Odom, M. L. Sulis, P. J. Real, A. Margolin, K. C. Barnes, J. O'Neil, D. Neuberg, A. P. Weng, et al. 2006. NOTCH1 directly regulates c-MYC and activates a feed-forward-loop transcriptional network promoting leukemic cell growth. [Published erratum appears in 2007 *Proc. Natl. Acad. Sci. USA* 104: 4240.] *Proc. Natl. Acad. Sci. USA* 103: 18261–18266.
51. Thompson, B. J., S. Buonamici, M. L. Sulis, T. Palomero, T. Vilimas, G. Basso, A. Ferrando, and I. Aifantis. 2007. The SCFFBW7 ubiquitin ligase complex as a tumor suppressor in T cell leukemia. *J. Exp. Med.* 204: 1825–1835.
52. O'Neil, J., J. Grim, P. Strack, S. Rao, D. Tibbitts, C. Winter, J. Hardwick, M. Welcker, J. P. Meijerink, R. Pieters, et al. 2007. FBW7 mutations in leukemic cells mediate NOTCH pathway activation and resistance to  $\gamma$ -secretase inhibitors. *J. Exp. Med.* 204: 1813–1824.
53. King, B., T. Trimarchi, L. Reavie, L. Xu, J. Mullenders, P. Ntziachristos, B. Aranda-Orgilles, A. Perez-Garcia, J. Shi, C. Vakoc, et al. 2013. The ubiquitin ligase FBXW7 modulates leukemia-initiating cell activity by regulating MYC stability. *Cell* 153: 1552–1566.
54. Tiedje, C., M. D. Diaz-Muñoz, P. Trulley, H. Ahlfors, K. Laaß, P. J. Blackshear, M. Turner, and M. Gaestel. 2016. The RNA-binding protein TTP is a global post-transcriptional regulator of feedback control in inflammation. *Nucleic Acids Res.* DOI: 10.1093/nar/gkw474.
55. Bogue, M. A., C. Zhu, E. Aguilar-Cordova, L. A. Donehower, and D. B. Roth. 1996. p53 is required for both radiation-induced differentiation and rescue of V(D)J rearrangement in scid mouse thymocytes. *Genes Dev.* 10: 553–565.
56. Dujka, M. E., N. Puebla-Osorio, O. Tavana, M. Sang, and C. Zhu. 2010. ATM and p53 are essential in the cell-cycle containment of DNA breaks during V(D)J recombination in vivo. *Oncogene* 29: 957–965.
57. Alt, J. R., A. Bouska, M. R. Fernandez, R. L. Cerny, H. Xiao, and C. M. Eischen. 2005. Mdm2 binds to Nbs1 at sites of DNA damage and regulates double strand break repair. *J. Biol. Chem.* 280: 18771–18781.
58. Rashkovan, M., C. Vadnais, J. Ross, M. Gigoux, W.-K. Suh, W. Gu, C. Kosan, and T. Möröy. 2014. Miz-1 regulates translation of Trp53 via ribosomal protein L22 in cells undergoing V(D)J recombination. *Proc. Natl. Acad. Sci. USA* 111: E5411–E5419.
59. Mendrysa, S. M., M. K. McElwee, J. Michalowski, K. A. O'Leary, K. M. Young, and M. E. Perry. 2003. mdm2 is critical for inhibition of p53 during lymphopoiesis and the response to ionizing irradiation. *Mol. Cell. Biol.* 23: 462–472.
60. Haks, M. C., P. Krimpenfort, J. H. van den Brakel, and A. M. Kruisbeek. 1999. Pre-TCR signaling and inactivation of p53 induces crucial cell survival pathways in pre-T cells. *Immunity* 11: 91–101.
61. Yu, Q., B. Erman, J.-H. Park, L. Feigenbaum, and A. Singer. 2004. IL-7 receptor signals inhibit expression of transcription factors TCF-1, LEF-1, and ROR-gammat: impact on thymocyte development. *J. Exp. Med.* 200: 797–803.
62. Boudil, A., I. R. Matei, H.-Y. Shih, G. Bogdanoski, J. S. Yuan, S. G. Chang, B. Montpellier, P. E. Kowalski, V. Voisin, S. Bashir, et al. 2015. IL-7 coordinates proliferation, differentiation and Tcr $\alpha$  recombination during thymocyte  $\beta$ -selection. *Nat. Immunol.* 16: 397–405.